5-2015

Postharvest Degradation of Microalgae: Effect of Temperature and Water Activity

Jacob A. Nelson
Utah State University

POSTHARVEST DEGRADATION OF MICROALGAE: EFFECT OF TEMPERATURE AND WATER ACTIVITY

by

Jacob A. Nelson

A thesis submitted in partial fulfillment
of the requirements for the degree

of

MASTER OF SCIENCE

in

Plant Science

(Crop Physiology)

Approved:

Dr. Bruce Bugbee Plant Physiology Major Professor	Dr. William J. Doucette Environmental Chemistry Committee Member
Dr. Lance C. Seefeldt Biochemsitry Committee Member	Dr. Mark R. McLellan Vice President for Research and Dean of the School of Graduate Studies

UTAH STATE UNIVERSITY
Logan, Utah

2015

Abstract

Postharvest Degradation of Microalgae:

Effect of Temperature and Water Activity

by

Jacob A. Nelson, Master of Science

Utah State University, 2015

Major Professor: Dr. Bruce Bugbee
Department: Plant, Soils and Climate

Algal postharvest degradation is an unexplored, yet key component of algalculture. We studied the effects of cold storage, water activity, pasteurization, and heat drying on lipids and protein degradation. Drying to a water activity between 0.90-0.95 a_w minimized triglyceride degradation for up to 30 days, but water activities above 0.96 or below 0.90 resulted in a more than 40% triglyceride degradation after 24 hours. Heating above 60° C via either drying oven or pasteurization for 1-3 hours prevented triglyceride conversion to free fatty acids, likely due to the deactivation of lipase. Lipid conversion to free fatty acids at temperatures between 55° C and 40° C averaged 10% per hour. Protein was stable between water activities of 0.45 and 0.99, but degraded 40% during a 60-minute pasteurization at 65° C. Arrest of enzymatic activity is critical to producing a stable algal product.

(98 pages)

Public Abstract

Postharvest Degradation of Microalgae:

Effect of Temperature and Water Activity

by

Jacob A. Nelson, Master of Science

Utah State University, 2015

Major Professor: Dr. Bruce Bugbee
Department: Plant, Soils and Climate

Though usually a nuisance in swimming pools and ponds, algae has the potential to be a valuable commodity for use as food and fuel. But before algae butter and biofuel become commonplace, issues with harvesting and storing this new crop need to be overcome. Though there has been ample research into how to grow and use algae, scientists have spent little time figuring out what to do after you pull it out of the water and before you eat it (or turn it into biodiesel). Algae, like all food products, starts to spoil as soon as it is harvested.

This study looked at three methods of preserving algae, freezing, drying, and pasteurization. Freezing is a good method for preserving fats and proteins, but it is expensive to freeze tons of algae. Freezing and thawing destroyed the algal cells, producing a soupy mixture that may cause complications for processing into foods or fuels. Drying was able to preserve the fats in algae, but only if it was dried just the right amount, about as dry as cheese or ham. Pasteurization was able to prevent the oils in the algae from going rancid by inactivating a protein in the algae that causes the oil to spoil rapidly.

Overall, this research is an initial step in finding a process to produce a shelf stable algal commodity, opening the door to new and valuable products for human use.

To my friend and partner Tiana.

Acknowledgments

I'm grateful to Lance Seefeldt for his biochemical knowledge and support of the algal program at USU. Also to Bill Doucette for his in-depth critical analysis, and for his personal mentorship. Neither this work, this degree, nor my career path would be possible if not for the leadership of Bruce Bugbee, who was willing to take a chance on me

I'd like to thank Peter Nelson and Saundra Rhodes for their detailed analytical work. Also, JaLene Hunt for her mastery of algalculture that kept that algae flowing. Alex McCurdy and Rhesa Ledbetter were paramount contributors to the biochemical analysis. Special thanks to Alec Hay for his excellent laboratory management and technical advice, and for hiring me.

I'd like to thank the members past and present of the crop physiology lab for their advice and friendship during my tenure, and my fellow graduate students Curtis Adams and Chris Perry for their for their technical and career advice. I am grateful to my faculty mentors, both official and casual, for investing their time on me.

I'm indebted to my family for their encouragement and support, including my siblings and grandparents. I'd like to thank Jeff and Debbie Hammer for their support during my time at USU. To my parents, listing the reasons for which I am grateful would take another thesis.

Jacob A. Nelson

Contents

Page

Abstract . . . **iii**

Public Abstract . . . **iv**

Acknowledgments . . . **vi**

List of Tables . . . **ix**

List of Figures . . . **x**

Acronyms and Symbols . . . **xii**

1 Introduction . . . **1**
1.1 Potential of algal bioproducts . . . 1
1.2 Algal farming . . . 3
1.2.1 Lipids, biofuels and beyond . . . 5
1.2.2 Protein . . . 6
1.3 Post-harvest stability . . . 6
1.3.1 Storage temperature . . . 7
1.3.2 Water Activity . . . 7
1.3.3 Pasteurization . . . 11
1.3.4 Effect of heat drying on bioproducts . . . 11
1.4 Objectives . . . 12

2 Materials and Methods . . . **13**
2.1 Algal culture . . . 13
2.2 Storage . . . 13
2.3 Freezing . . . 13
2.4 Water activity and moisture content . . . 14
2.5 Lyophilization . . . 15
2.6 Incubation . . . 15
2.7 Heat drying . . . 15
2.8 Respiration . . . 16
2.9 Pasteurization . . . 16
2.10 Protein analysis . . . 16
2.11 Free amino acid analysis . . . 17
2.12 Extraction and transesterification for FAME analysis . . . 17
2.13 Extraction of triglycerides and free fatty acids . . . 17
2.14 GC analysis . . . 18

3 Results and Discussion **19**
3.1 Algal biomass characterization 19
3.2 The effect of freezing on membrane integrity and cell degridation 19
3.3 Water activity 21
3.3.1 Relationship of water content to water activity. 21
3.3.2 Effect of water activity on respiration. 22
3.3.3 Effect of water activity on algal bioproducts 22
3.4 Pasteurization 27
3.4.1 Effect of pasteurization on respiration 27
3.4.2 Effect of pasteurization on algal bioproducts 27
3.5 Hot air drying 29
3.5.1 Effect of hot air drying on algal bioproducts 29
3.6 Deactivation of lipase 35
3.7 Composition of non-FFA producing TAG degridation 36

4 Conclusions **37**
4.1 Freezing and chilling 37
4.2 Protein as a nutritional product 37
4.3 Lipids 38
4.4 Energy and cost of lipase deactivation 38
4.5 Further research 39
4.6 Final remarks 39

References **40**

Appendices **43**
A Economic Analysis of Greenhouse Lighting: Light Emitting Diodes vs. High Intensity Discharge Fixtures 44
A.1 Introduction 44
A.2 Materials and Methods 51
A.3 Results 52
A.4 Discussion 53
A.5 Conclusions. 58
Appendix A References 62
B Analysis of environmental effects on leaf temperature under sunlight, High Pressure Sodium and Light Emitting Diodes 64
B.1 Introduction 64
B.2 Materials and Methods 67
B.3 Results and discussion 74
B.4 Conclusions 80
B.5 Supporting Information 81
Appendix B References 84

List of Tables

Table Page

1.1 Pasteurization time and temperature for milk 12

2.1 Pasteurization times and temperatures 16

A.1 Efficiency of individual LEDs at a drive current of 700 mA 48

A.2 Efficiency of fixtures using integrating sphere measurements compared with flat-plane integration 59

A.3 Photon efficiency and cost per mole of photons, assuming all photons (180°) are captured by plants 60

A.4 Cost per mole photons for four capture assumptions 61

B.1 Incident radiation, fraction absorbed, and total absorbed radiation for each source 78

List of Figures

Figure Page

1.1 Algal research and oil prices over the last fifty years 2

1.2 The rapid rise in palm oil production 6

1.3 Conceptual diagram of the effect of water activity on biochemical reactions . 8

1.4 Hydrolysis of triglycerides to free fatty acids 9

2.1 USU Flat plate bioreactors 14

2.2 Jars of algal biomass at various water acitivity levels for incubation 15

3.1 The effect of freezing on *Scenedesmus dimorphus* 20

3.2 The effect of freezing *Scenedesmus dimorphus* on EC 21

3.3 Moisture desorption isotherm of *Scenedesmus dimorphus* 22

3.4 Algal degradation as a function of water activity 23

3.5 Effect of water activity on algal bioproduct degradation after 30 days 24

3.6 Algal bioproduct degradation rate over time at various water activities 25

3.7 Sample GC response 28

3.8 The evolution of CO_2 after pasteurization of algal slurry samples 29

3.9 Effect of pasteurization temperature on degradation of bioproducts 30

3.10 Effect of pasteurization time on degradation of bioproducts 31

3.11 Sample temperature during hot air drying 32

3.12 Algal bioproduct degradation as a function of drying oven air temperature . . 33

3.13 Algal bioproduct degradation rate after drying for different time periods . . . 34

A.1 The photon distribution of four fixtures with similar photon efficiency 46

A.2 Canopy photon capture efficiency 47

A.3 Yield photon flux curve 49

A.4 Effect of drive amperage and color on photon efficiency of LEDs 50

A.5 Effect of electricity price on average annual cost over five years for two capture scenarios 54

A.6 Effect of canopy capture efficiency on average annual cost over five years . . . 55

B.1 Transmission of radiation through a single pane of tempered glass 66

B.2 Average absorption (red line) of leaves from tomato, pepper, basil and broccoli 68

B.3 Radiance spectrum from four radiation scources and average leaf absorbance . 69

B.4 Leaf temperature response to air temperature 75

B.5 Radiance spectrum from four radiation scources and average leaf absorbance . 76

B.6 Calculated effects of PPF on the difference between leaf temperature and air temperature under four radiation scenarios in near worst-case conditions of water stress and low wind 77

Acronyms and Symbols

a_w	water activity
p	vapor pressure
p_0	saturation vapor pressure of pure water
FFA	free fatty acids
FAME	fatty acid methyl esters
TAG	triacylglyceride or triglyceride
FAA	free amino acids
EC	electrical conductivity
V_w	molar volume of liquid water
T	temperature
R	ideal gas constant
TCA	trichloroacetic acid
BSA	bicinchoninic acid
GC	gas chromatograph
FID	flame ionization detector
LED	light emitting diode
HPS	high pressure sodium
HID	high intensity discharge
CMH	ceramic metal halide
PPF	photosynthetic photon flux
YPF	yield photon flux
UV	ultra violet
NIR	near infrared radiation
PAR	photosynthetic active radiation

Chapter 1

Introduction

1.1 Potential of algal bioproducts

It is estimated that algae contribute approximately 46% of global net primary productivity, at nearly 50 petagrams ($10^{12}\,g$) of carbon per year (Field et al., 1998), yet it is virtually unutilized by humans. Generally this underutilization comes from a historical lack of economically viable protocols for large scale algal cultivation. Factors such as designing infrastructure, providing adequate growing conditions, preventing competitive species, and harvesting have all proven difficult hurdles to overcome, especially on large scales. While agriculture goes back thousands of years, the first attempts of algaculture were reported only about 120 years ago (Bold, 1942).

Commercial applications for algae have been limited to use as feed for farmed mollusks, and larvae of prawns, fin-fish and crustaceans (Borowitzka, 1997). However, the majority of recent research in algae has been for use in biofuels, with hundreds of algae companies having formed over the last decade to capitalize on this new market and large investments coming from both the private and public sector (Pienkos and Darzins, 2009). A spike in oil prices around 2005 correlated with an exponential increase in algal biofuels research (Fig. 1.1).

In one of the most highly cited papers in the field, Chisti (2007) projected that algae has the potential to produce over 130 $^{m^3\,oil}/_{ha\cdot yr}$, as compared to the next highest producing land crop, oil palm at about 6 $^{m^3\,oil}/_{ha\cdot yr}$. This projection is based on extrapolation of lab scale experiments, and likely vastly overestimates the actual potential. Quinn et al. (2012), in a pilot scale experiment done over two years with CO_2 enrichment, found average annual fatty acid methyl esters (FAME, or biodiesel) productivities of 9.9 to 13.1 $^{m^3\,oil}/_{ha\cdot yr}$, which

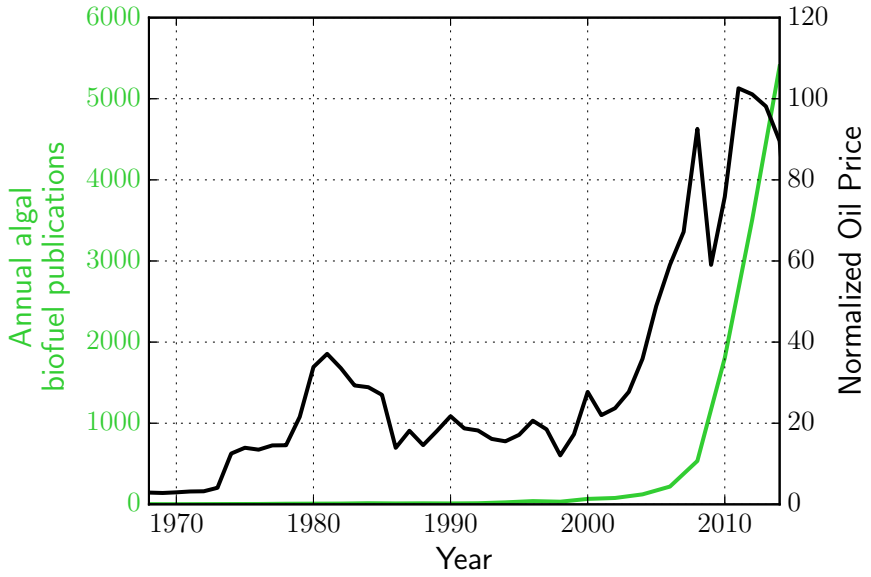

Fig. 1.1: **Algal research and oil prices over the last fifty years.** Algal biofuel research measured as hits to the keywords "algae biofuel" on Google Scholar (google.scholar.com, accessed April 2015). Nominal oil price is the inflation adjusted price of crude oil imports, data from U.S Energy Information Agency Real Petroleum Prices (http://www.eia.gov/forecasts/steo/realprices/, accessed April 2015).

is consistent with typical production rates at Utah State University at 8 to 16 $^{m^3\,oil}/_{ha\cdot yr}$ (unpublished data), also with CO_2 enrichment (CO_2 enrichments is further discussed in section 1.2). So while algal productivities may have been exaggerated in the past, it has been demonstrated to be a productive crop.

Aside from impressive productivity, algal cultivation does not require arable soil and could be produced on marginal and currently non-productive lands. Field et al. (2008) and Campbell et al. (2008) estimated 386 and 472 Mha respectively of global abandoned agricultural lands, which would translate to about 4 billion metric tonnes of algal oil without impacting current food supplies, if all land was used for intensive, CO_2 enriched algal farming.

Land will not likely be the limiting factor for algal production. Water use in algal production is likely to be higher than that found in land plants, as land plants use stomates to regulate transpiration. This effect may be partly offset by higher yields from CO_2 supplementation, which can increase yields without increasing water use. Algae is also unique

in that many productive species, such as species from the genus *Nannocholopsis*, utilize salt water. Using saline or brackish waters allows for crop production with little impact on fresh water supplies.

Hydroponic algal production can also prevent nutrient leaching. Precision nutrient management, as well as reuse of media, allows for high nutrient use efficiencies and less environmental impacts downstream. Clarens et al. (2010) estimates that algal production could reduce eutrophic discharge by 85% when compared to traditional corn and canola. Algae is already used as a means for wastewater treatment, and coupling algal production with waste water treatment facilities could decrease the need for inorganic fertilizers as well as provide a valuable byproduct (Pittman et al., 2011).

1.2 Algal farming

Algal culture consists of three main phases: inoculation, growth, and harvest. The inoculation phase consists of generating sufficient inoculum from axenic seed monocultures. Single strain seed cultures for inoculation are maintained in an exponential growth phase until needed. Current research has focused on 10-20 key species, including Cyanobacteria and three classes of eukaryotic of algae: Chlorophytes (green algae), Bacillariophyceae (diatoms), and Eustigmatophyceae (Rodolfi et al., 2009). Algae are a diverse, polyphylitic group, and characteristics as to their relative cultivability on large scales and the products of interest they produce varies considerably. Maintaining the desired genetic composition can prove difficult on large scales, so while inoculum can be used from previous production batches (Quinn et al., 2012), species drift over time warrants that axenic monocultures be maintained. Strains are selected for the desired application, keeping in mind factors such as salinity tolerances, product of interest (lipids, proteins, vitamins, etc.), productivity, nutrient needs, and culture stability.

Growth

The majority of biomass and bioproduct is accumulated during the growth phase. Content of products of interest is influenced by culture conditions, particularly environmental

stresses, so precise nutrient and cultural management allow for greatly improved productivities (Adams et al., 2013). Culture health depends on well regulated environmental conditions, the key factors being temperature, pH and light levels.

Supplemental CO_2

pH is generally controlled via CO_2 gas injection, which also acts to increase growth rates. Flue gas has been proposed to supply the large amounts of CO_2 required for supplementation. Quinn et al. (2013) concluded that the distance from a CO_2 supply was a hard economic limit to algal production, leaving only 0.28 Mha of suitable land within 4.8 km of a CO_2 source, or less than 0.5% of available barren land . Though CO_2 supplementation may be a barrier in algal production, it is also a unique benefit, as CO_2 supplementation of traditional crops is difficult without expensive controlled environments.

Harvest

The harvest stage consists primarily of dewatering the algae. The energy to remove water increases exponentially as the water content decreases. Xu et al. (2011) found that between 18-90% of the energy expenditure to produce algal biofuel was in the drying phase, depending on the drying method. Algal cultures range between 0.5 and 5 grams per liter at peak density. The initial dewatering step takes the density to around 1-10% solids, via flocculation, filtration or centrifugation, resulting in an algal slurry. The next stage involves taking the algal slurry to an algal paste of about 10-40% solids, generally via centrifugation.

Dewatering steps have been well examined and reviewed, and various methods of filtration, flocculation, sedimentation and centrifugation having been tested on algae (reviewed by Borowitzka and Moheimani, 2013) Sharma et al. (2013), Milledge and Heaven (2012), and Uduman et al. (2010) all concluded that flocculation has potential as the most energy efficient dewatering technique, while Molina Grima et al. (2003) advised that centrifugation would be most suited when harvesting algae for high value products. Show et al. (2013) concluded that all current dewatering techniques had significant disadvantages that needed to be overcome. The reviews agree that there is no one best method for every situation, and

that further reductions of dewatering costs and energy consumption are critical for viable algal commercialization.

1.2.1 Lipids, biofuels and beyond

The potential use of microalgae for the production of oil, especially for biofuels, has been reviewed and scrutinized ad nauseam over the last decade (see Brennan and Owende (2010) as one example). Generally, algal triglycerides are extracted and transesterified, producing FAME (biodiesel) (Wahlen et al., 2011). In a later paper, Wahlen et al. (2013) found that microbial biofuels combusted in an engine performed similarly to a traditional soybean base biodiesel, with the C16 rich algal biodiesel from *Chaetoceros gracilis* producing emissions with reduced NO_x pollutants.

Aside from good quality biodiesel, oils rich in short chain, C16 lipids, are used in the cosmetic industry, produce good quality detergents and also have favorable characteristics as a food ingredient. Current sources of oils rich in C16 lipids are tropical plants such as coconut and, primarily, oil palm. Figure 1.2 shows the steady increase of global palm oil production over the last decade.

The majority of palm oil production comes from Southeast Asia, with 85% of the global production in 2009 coming from Malaysia and Indonesia (Food and Agriculture Organization of the United Nations; fao.org, accessed Jan 2014). Oil palm has been implicated as a factor in deforestation in this region, which may exacerbate species diversity loss and extinction (Fitzherbert et al., 2008). Deforestation and destruction of peat bogs for oil palm plantations has also been projected to release large amounts of CO_2 into the atmosphere, contributing to global warming (Hooijer et al., 2010).

Short chain lipids, such as C16 triglycerides, are produced in high amounts by both the Bacillariophyceae (diatoms) and Eustigmatophyceae (Brown et al., 1997). Species from both these groups pose the possibility to produce short chain lipids in temperate climates, with less environmental impact.

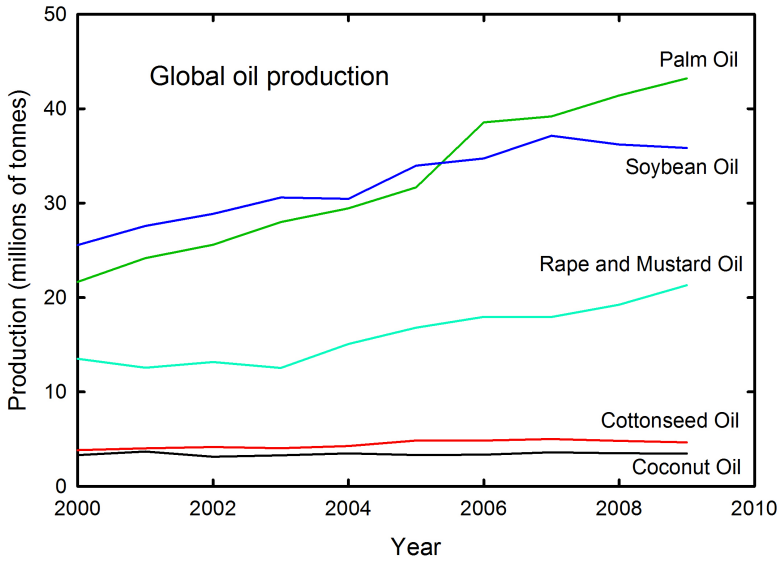

Fig. 1.2: **The rapid rise in palm oil production.** Demand for palm oil has increased dramatically over the last decade. Data from the Food and Agriculture Organization of the United Nations (fao.org, accessed Jan 2014).

1.2.2 Protein

While the promise of biofuels has driven research on algal lipid production, the promise of algal proteins has gone relatively unexplored. In an analysis by Becker (2007), protein compositions greater than 50% by weight were found in a variety of species. In addition to the high protein content, algal proteins were found to have a good net protein utilization (Becker, 2004), similar to those found in whole grains and legumes, indicating that the protein is of good quality. The largest hurdles for algal protein are the same as for algal food lipids: adoption, palatability, and costs.

1.3 Post-harvest stability

Algae, like all agricultural crops, needs to produce stable products that can be stored and shipped. Most modern reviews of algal production assume little to no storage time of the harvested algal product, assuming instead that the algae will be processed immediately after harvest. This assumption would require extraction and processing facilities at the growing site that could accommodate the peak summer volume of algal production. As Quinn et al.

(2012) demonstrated in a temperate climate, peak summer algal production may be two to three times greater than average annual production and, therefore, a coupled processing facility with no storage capability would be overbuilt by a factor of two to three. A stable algal product is paramount to the use of algae as a feedstock.

Algal paste is not a stable product and all components will degrade, generally starting with high value storage compounds such as lipids and specialty products such as vitamins. Prevention of spoilage requires the arrest of unwanted enzymes, organisms and reactive species. Little work has been done on the spoilage of algal products post-harvest, but parallels can be made to well-studied fields of microbial metabolism and food science.

1.3.1 Storage temperature

In the study of algal bioproducts, the testing of samples is often temporally separated from the production facilities. The effect of delays in measurements may have significant impacts on the physiological and biochemical properties of algal biomass. Letting algal samples sit at room temperature for prolonged periods of time allows metabolic and microbial degradation. Conversely, freezing, while maintaining important compounds like lipids and proteins, can reduce cell viability (Cordero and Voltolina, 1997), which may cause problems in down stream processes such as centrifugation and filtration.

1.3.2 Water Activity

In food science, due to it's good correlation to product stability, water content is measured as water activity (a_w), which is defined as

$$a_w = \frac{p}{p_0} \tag{1.1}$$

where p is the vapor pressure of the water in the substance and p_0 is the vapor pressure of pure water at the same temperature. This equation is the same as the equation for relative humidity, and the water activity of a sample is equal to the equilibrium relative humidity of the air surrounding the sample in a closed chamber. Water activity quantifies the energy

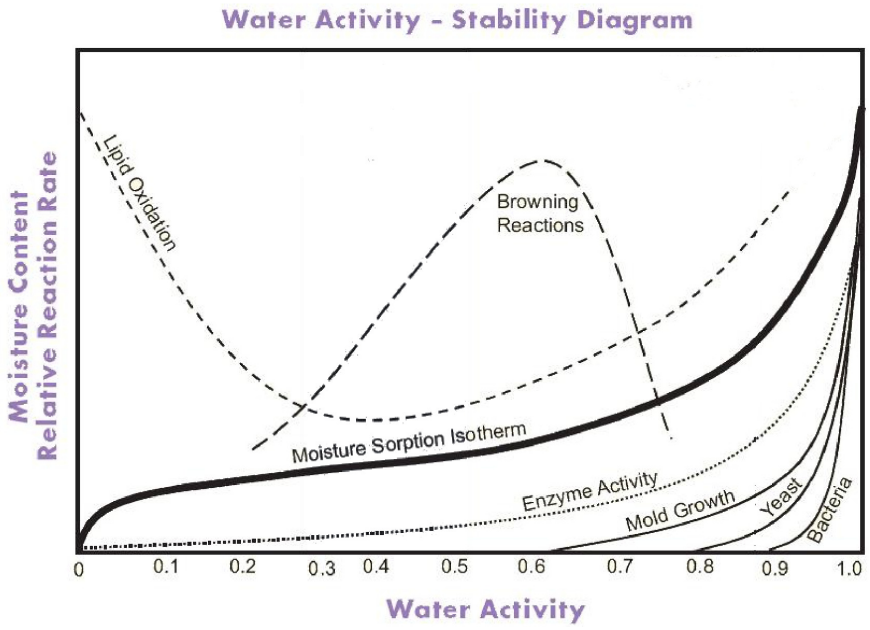

Fig. 1.3: **Conceptual diagram of the effect of water activity on biochemical reactions.** Adapted from http://devfr.aqualab.com/enseignement/water-activity-for-product-safety-and-quality/, accessed January 2009.

status of the water in a system and can be conceptualized as the degree to which the water is "bound," where "bound water" is less likely to be used as a reactant or solvent. As water activity decreases, hydrophobic, lipophilic reactions increase while hydrophilic and aqueous-diffusion-limited reactions, such as many enzymatic reactions, decrease. Figure 1.3 shows the relationship between water activity and some key chemical and biological activities.

Microbial degradation

Microbes are the most significant source of degradation at high water activities (>0.9 a_w). Most bacteria will stop growing at water activity levels lower than 0.9, with most molds and yeasts severely inhibited at activities below 0.7-0.8. The limit for biological activity is considered to be a water activity of 0.6. The United States FDA considers food with a water activity level less than 0.85 to no longer be classified as a "potentially hazardous food", due to the inhibition of harmful microorganisms.

In addition to microbial spoilage, stored algae is subject to chemical degradation, including hydrolysis, oxidation and Maillard reactions. Like microbial growth, chemical stability

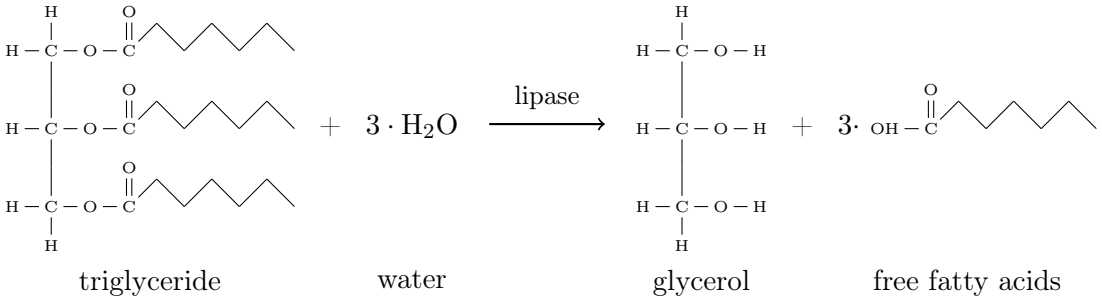

Fig. 1.4: **Hydrolysis of triglycerides to free fatty acids**

correlates better with water activity than it does moisture content.

Hydrolysis

Hydrolysis is the cleavage of chemical bonds by the addition of water, which is generally catalyzed by enzymes in biological systems. Hydrolysis is the first step in many degradation pathways, as it breaks large molecules into smaller components. In the case of lipids, hydrolysis, facilitated by lipase, cleaves the fatty acid chains of neutral storage lipids (triglycerides) to form free fatty acids (Fig. 1.4). Lipid hydrolysis gives oils rancid characteristics, which is undesirable for food products. Ramadhas et al. (2005) found that free fatty acid content also had a negative effect on biofuel production, as the traditional alkaline catalyst transesterification was significantly inhibited. In a review of FAME production processes, Vyas et al. (2010) recommended free fatty acid contents no greater than 3%.

Chen et al. (2012) found that algal lipids from *Scenedesmus sp.* paste went from 72% to 4% triglycerides (triacylglycerides, or TAG), while free fatty acids increased from non detectable levels to 70%, in just one day at room temperature. This degradation was likely the result of lipase catalyzed hydrolysis in the wet algal paste. Though lipases from various species have been shown to be active at nearly all water activities in organic solvents (Wehtje and Adlercreutz, 1997), they can be slowed significantly at moderate water activities due to limited molecular mobility and the availability of water as a reactant (Troller, 2012). Hydrolysis of proteins, or proteolysis, results in smaller peptides and/or amino acids, which effect protein function, but have a small impact on bioavailability and nutrition.

Oxidation

Lipid oxidation occurs via the formation of free radicals, which then sets off a self-propagating cascade of chemical reactions, resulting in degradation, off-flavors, and unwanted byproducts. Propagation of the reaction requires the presence of oxygen, and therefore aerobic conditions. Oxidation rates depend both on the initial chemical composition of the substance, and environmental conditions. Rates increase in the presence light and transition metals such as iron and zinc. Unsaturated fatty acids are more prone to oxidation, and therefore saturated fatty acids tend to be more oxidatively stable, even after being transesterified to biodiesel. Lipid oxidation decreases with increasing water activity until it reaches a minimum around 0.3-0.6 a_w, above which it begins to increase again (see Fig. 1.3). Oxidation at high water contents is based on the degree to which oxygen can dissolved and the activity of antioxidants. Not only does oxidation degrade triglycerides, but lipid free radicals can also combine with and break down proteins. Therefore, even oxidation of low lipid samples should be avoided.

Preventing oxidation can be accomplished by removing oxygen, via vacuum or by replacing it with an inert gas, or by terminating the radical cascade using antioxidants. Antioxidant activity generally increases with increasing water activity as the antioxidants become more soluble. Oxidation is a complex process and can be difficult to predict.

Maillard reactions

Maillard reactions are the principle, non-microbial degradation route of proteins. Maillard reactions are a type of browning reaction, named after the brown colors they give foods. In particular, Maillard reactions give bread crust it's color and aromatic characteristics, and are the result of a combination of amino groups and reducing sugars which can occur with or without enzymes. Maillard reactions take complex pathways with varying end products, but the net result is a reduction of protein suitable for human consumption. Moderate water contents facilitate Maillard reactions, which peak around 0.6-0.7 a_w (see Fig. 1.3).

Water activity levels for preservation

Generally, foods at a water activity around 0.2-0.3 are considered to be the most stable, but intermediate water activities (0.6-0.9 a_w) may provide a compromise between minimizing the energy used to remove water and protection from degradation.

1.3.3 Pasteurization

Pasteurization inactivates enzymes and is thus another potential means to inhibit both microbial and chemical degradation. Without pasteurization, Chen et al. (2012) found that after 4 days of storage at 4° C, 85% of the relatively high value algal triglycerides (TAG) were converted to free fatty acids with little degradation of total lipid content. This suggests enzymatic lipid degradation via lipase, rather than microbial degradation or metabolism. Pasteurization may be an effective method of preventing enzymatic degradation. Heating to moderate temperatures ($< 100°$ C) for short time periods (< 60 minutes) will unfold many enzymes and leave them inactive without significant degradation of other bioproducts. This technique has been used in the food industry for many years, and has been proven to significantly stabilize products such as milk, allowing them to be stored for months or even years. Table 1.1 gives an overview of the recommended pasteurization temperatures and times for dairy products.

1.3.4 Effect of heat drying on bioproducts

In contrast to the wet heat of pasteurization, which unfolds and inactivates proteins, drying can make proteins more resistant to heat. When trying to preserve enzymes, drying can prevent denaturation of proteins by limiting their capacity to unfold (Troller and Christian, 1978). Turner et al. (1995) found the denaturation temperature of liver carboxylesterase to increase as a function of decreasing water activity, by as much as 50° C in anhydrous conditions. Because enzyme functions can be preserved, unwanted reactions could continue to take place at slow rates in samples that have been dried at low temperatures.

Maillard reactions are significantly increased at high temperatures, as seen when heating food. This effect is most prominent at lower water activities.

Table 1.1: Pasteurization time and temperature for milk as outlined in the Grade "A" Pasteurized Milk Ordinance (Public Health Service/Food and Drug Administration 2009).

Pasteurization

Temperature	Time
66° C	30 minutes
75° C	15 seconds
89° C	1.0 second
90° C	0.5 seconds
94° C	0.1 seconds
96° C	0.05 seconds
100° C	0.01 seconds

Mild heating for short periods has small effects on lipid oxidation, though high heat ($>$ 100° C) and longer periods of high heat promote lipid oxidation. Thomsen et al. (2005) found evidence of significantly increased lipid oxidation in whole milk powders when stored at 45° C as compared to 35° C, though the effect was minimal within the first 30 days.

1.4 Objectives

The objective was to find effective postharvest treatments to minimize lipid and protein degradation, focusing on freezing, water activity, pasteurizing, and heat drying.

Chapter 2

Materials and Methods

2.1 Algal culture

Scenedesmus dimorphus (UTEX #417) was used in this analysis due to it's high biomass productivity and consistent output of lipids and proteins. Both high and low nitrogen treatments were grown to insure the presence of both proteins and storage lipids. Cultures were grown in 130 liter flat plate bioreactors, continuously mixed via airlift, and controlled for temperature (flat plate bioreactors shown in Fig. 2.1). Media was controlled at a pH of 7.5 via CO_2 enrichment. Supplemental lighting from HPS fixtures maintianed a minimum PPF of 500 $^{\mu mol}/_{m^2 s}$ for a photoperiod of 16 hours (see appendices A and B for more information on supplemental plant lighting).

Freshwater media for *Scenedesmus dimorphus* was composed of 0.19 grams per liter of commercial 5-11-26 hydroponic fertilizer (Peters Professional Hydro-Sol, The Scotts Company, Marysville, OH, USA), supplemented with 0.2 mM $MgSO_4$, 0.45 mM $CaCl_2$, 4.6 µM DTPA-Fe, and either 6.5 or 4.3 mM KNO_3 for high and low nitrogen treatments.

Algal biomass was harvested to approximately 10% solids using tangential flow microfiltration, and further dewatered via centrifugation to about 25% solids.

2.2 Storage

All samples for protein analysis were stored at -20° C until analysis. All samples for lipid analysis were lyophilized and stored at -80° C until analysis.

2.3 Freezing

Samples of previously unfrozen *Scenedesmus dimorphus* algal slurry (approximately 10% solids) were homogenized and characterized via electrical conductivity (EC) and viewed

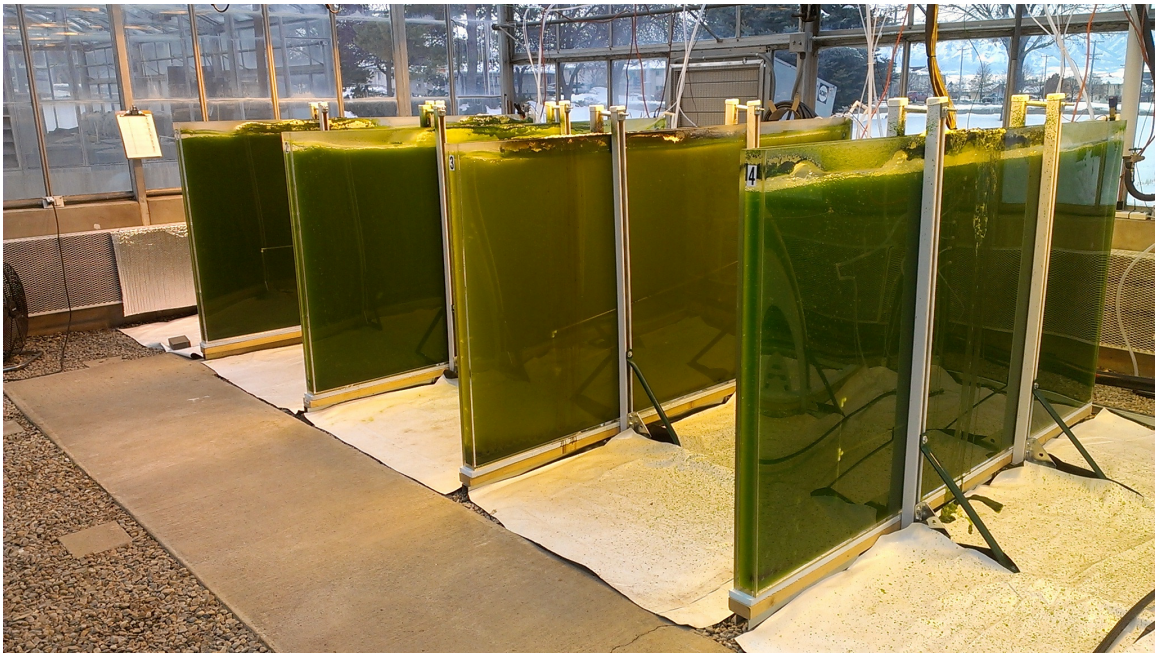

Fig. 2.1: **USU Flat plate bioreactors.**

under the microscope. Electrical conductivity measures extracellular solutes, and an increase in EC corresponds to leaking of cellular contents, and thus membrane damage. Samples of 25 ml were placed in 0.5 L jars, then sealed and placed into one of four storage temperatures: -80°, -15°, 4° and 25° C. After 24 hours in storage, each sample was defrosted and again analyzed for EC and viewed under the microscope.

2.4 Water activity and moisture content

Moisture content was determined by ratio of wet weight and weight after drying in a drying oven. Water potential was measured using a dew point potentiometer (WP4C, Decagon Devices, Pullman, WA, USA) and converted to water activity using the formula,

$$a_w = e^{V_w p / RT} \tag{2.1}$$

where a_w is the water activity, V_w is the molar volume of liquid water, p is the vapor pressure of the sample being measured, T is temperature in kelvin, and R is the ideal gas constant.

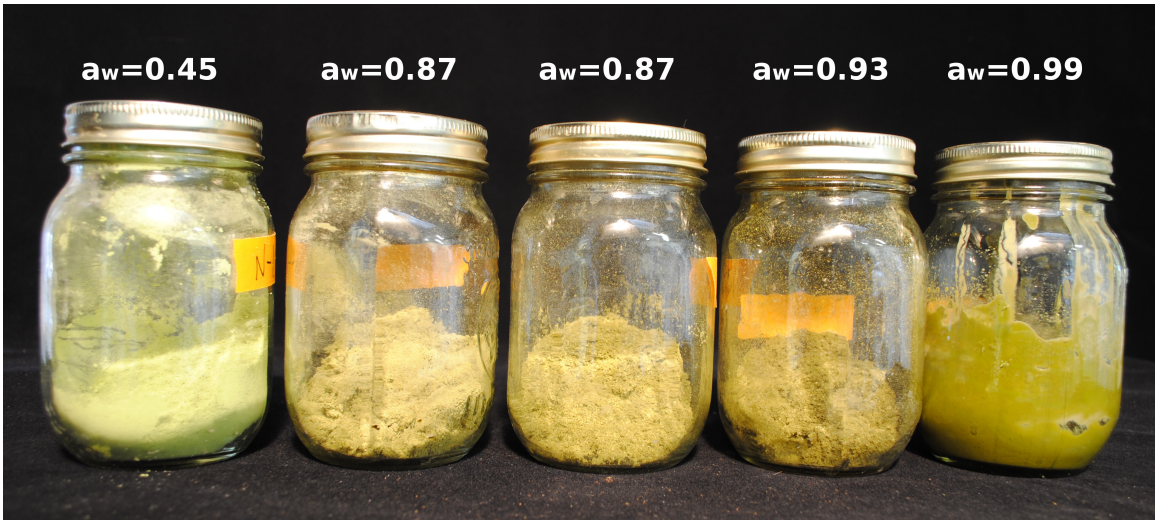

Fig. 2.2: **Jars of algal biomass at various water acitivity levels for incubation.**

2.5 Lyophilization

Centrifuged samples (approx. 15-30% solids) were frozen at -80° C, then lyophilized until thoroughly dry, forming a light powder. Lyophilization generally took 1-3 days depending on sample thickness. Samples that were partially dried were periodically sampled for water activity during lyophilization. Once the desired water activity was met, samples were placed back in -80° C storage.

2.6 Incubation

Samples were incubated in Mason jars, with lids sealed when CO_2 measurements were taken, otherwise left loose to allow for gas expulsion. Fig. 2.2 shows jars of algal biomass at various water activity levels that were incubated. Incubated samples were not agitated and kept in darkness at a temperature controlled 24° C.

2.7 Heat drying

Heat dried samples were placed in temperature controlled drying ovens at either 75° C or 55° C. Drying oven and sample temperatures were monitored via thermocouple connected to a datalogger. Samples depths were approximately 0.5 cm in cylindrical plastic discs with a diameter of 4 cm. Water activity was periodically monitored by removing a sample and

measuring as indicated in section 2.4

2.8 Respiration

Samples for respiration were sealed in 1-liter Mason jars fitted with a rubber septum in the lid, allowing for sampling of head space gas via syringe. The head space was periodically sampled and analyzed for CO_2 using an infrared gas analyzer (model 6250, LICOR, Inc., Lincoln, NE, USA). Samples were left undisturbed during incubation and sampling without flushing the head space to mimic storage conditions.

2.9 Pasteurization

500 ml samples of algal slurry (about 10% solids) were heated in a 600 ml beaker on a hot plate with continuous stirring to the desired temperature and held for the alloted time as outlined in Table 2.1. Samples were immediately cooled to room temperature after pasteurization in an ice bath. Once cooled, samples were immediately placed in cold storage until analyzed. Three times and temperatures were used.

Table 2.1: Pasteurization times and temperatures.

Pasteurization

Temperature	Time
66° C	30 minutes
75° C	15 seconds
90° C	0.5 seconds

2.10 Protein analysis

Protein samples consisted of 30 ml of 1 molar sodium chloride containing 200 mg of algal cells, which was homogenized and lysed via French pressure cell press (SLM Aminco French Pressure Cell Press Model FA-078, Urbana, IL, USA). Lysed samples were stored at -20° C until they were measured. Once thawed, a 1 ml subsample was mixed with 0.2 ml of 3.6 mM deoxycholate, followed by an addition of 0.2 ml of 4.4 M trichloroacetic acid (TCA) and vortex mixing. TCA/algal mixtures were held at room temperature for 10 minutes to

allowed protein to precipitate, after which the sample was centrifuged and decanted, with the supernatant collected and stored for free amino acid analysis (see section 2.11). Two milliliters of 4% sodium dodecyl sulfate was added to the protein precipitates and the solution was heated in a boiling water bath for 15 minutes to bring the protein back into solution. Protein was quantified using a commercial BCA protein assay kit (Pierce Biotechnology), using bovine serum albumin as a standard, and measured with a spectrophotometer at 562 nm.

2.11 Free amino acid analysis

Free amino acids were quantified by measuring the fluorescence resulting from the reaction of fluorescamine with amino acids. One mL of supernatant from the protein precipitation (see section 2.10) was combined with 3 ml of 200 mM sodium borate buffer. The amino acid solution was then combined with 1 ml of a 0.5 mM solution of fluorescamine in acetone and thoroughly mixed. Florescence was measured at 480 nm with an excitement wavelength of 390 nm, and amino acids were quantified against a standard curve of glutamate. The use of this method on algal samples is further discussed and evaluated in Clayton et al. (1988).

2.12 Extraction and transesterification for FAME analysis

All samples were analyzed for three lipid components: triacylglycerides (TAG), free fatty acids (FFA), and total tranesterifiable lipids as fatty acid methyl esters (FAME). Lyophilized algal samples (100 mg) were transesterified in 2 ml of a 1.8% (v/v) mixture of methanol and sulfuric acid at 80° C for 1.5 hours, mixing every 15 minutes. Immediately following transesterification, samples were thrice extracted in chloroform, homogenized, and stored at -80° C until GC analysis. FAME was quantified against a standard curve composed of equal parts methyl myristate, methyl palmitoleate, and methyl oleate.

2.13 Extraction of triglycerides and free fatty acids

TAG and FFA lipids were extracted using a modified Bligh and Dyer extraction. A 200 mg sample of lyophilized algae was mixed with 4 mL of a 2:1 volumetric ratio of chloroform

to methanol. The algal solution was then sonicated continuously for 30 seconds, followed by a wash with water, centrifugation, and removal of the aqueous phase. This extraction was repeated 3 times total and the resulting chloroform solution was homogenized. Free fatty acids were conjugated by adding MSTFA (N-Methyl-N-(trimethylsilyl) trifluoroacetamide) and allowed to sit at room temperature for 30 minutes. All extracted samples were stored at -80° C until GC analysis. Free fatty acids were quantified against a standard curve of equal parts Myristic, Palmitic, and Stearic acids. Triglycerides were quantified against a standard curve of Tripalmitin.

2.14 GC analysis

All lipid samples were analyzed via gas chromatography (Model 2010, Shimadzu Corporation) coupled with a flame ionization detector (FID). Analytes were separated in a RTX-Biodiesel column (Restek, Bellefonte, PA, USA). The column temperature program was 1 minute at 60° C, followed by a ramp up of 10° C per minute to 360° C, then held for 6 minutes. Helium was used as a carrier gas at 50 $^{cm}/_{s}$. The FID was set to 380° C, and output was post-processed by peak area integration. All samples were compared to the standards described in sections 2.12 and 2.13 by linear regression. Responses between retention times of 9-19 minutes were counted as FAME in the transesterified samples and FFA in the Bligh and Dyer samples. Responses between retention times of 31-36 minutes were counted as TAG in the Bligh and Dyer samples.

Chapter 3

Results and Discussion

3.1 Algal biomass characterization

Five replicate samples from both the high and low nitrogen algal cultures were analyzed to obtain a baseline algal component characterization. Inital algal protein content was 172±16 $^{mg}/_{g\,biomass}$ for the high nitrogen cultures and 140±25 p $^{mg}/_{g\,biomass}$ for the low nitrogen cultures. Initial total free amino acid content was low in both cultures with an average of 54±6 $^{\mu g}/_{g\,biomass}$ for both high and low nitrogen cultures. FAME contents were similar between the two cultures, with 310±20 $^{mg}/_{g\,biomass}$ in the high nitrogen cultures and 344±19 $^{mg}/_{g\,biomass}$ in the low nitrogen cultures. TAG content was lower in the high nitrogen compared to the low nitrogen cultures, with 88±23 and 130±17 $^{mg}/_{g\,biomass}$ respectively. Free fatty acid contents were similarly low, with 104±3 and 145±8 $^{mg}/_{g\,biomass}$ in the high and low nitrogen cultures respectively.

Protein measurements were influenced by treatments, sometimes giving results higher than original levels. This effect was likely due to either the increase in cellular digestibility, allowing more protein to be quantified after treatments, or also influences in pH. Protein trends may still be a valid if the treatments were all similar, which assumes no overall bias.

3.2 The effect of freezing on membrane integrity and cell degridation

Figure 3.1 shows *Scenedesmus dimorphus* cells before and after freezing at -80° C. Frozen cells did not maintain colonies and appear to have lost some cellular contents, indicating that the cell membranes have been physically damaged. Freezing did not appear to completely lyse *Scenedesmus dimorphus* cells (Fig. 3.1B). The freezing process is known to shear cells (Karlsson and Toner, 1996), and likely broke up colonies of *Scenedesmus dimorphus*.

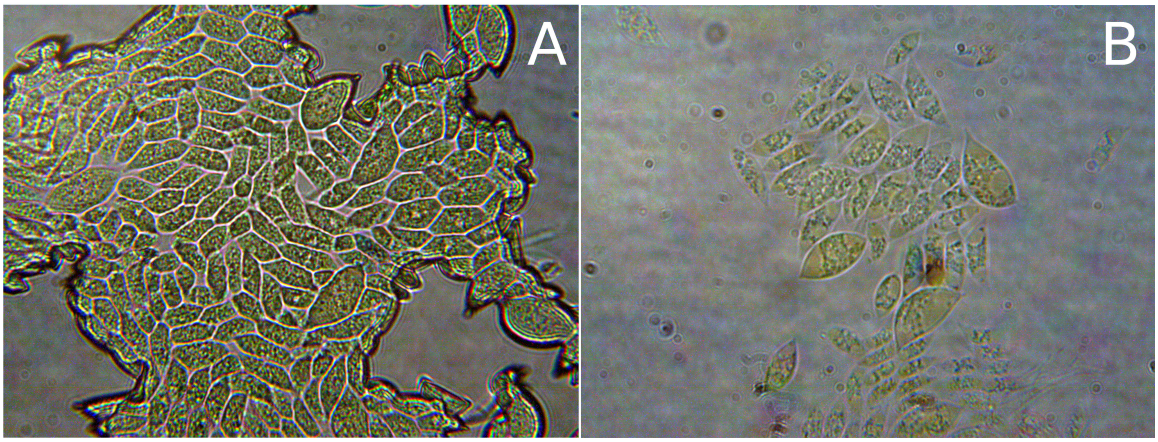

Fig. 3.1: **The effect of freezing on *Scenedesmus dimorphus* A** Before freezing, cells stick together in colonies and appear full. **B** After freezing at -80° C, cells no longer form robust colonies and appear partially emptied.

Freezing increased electrical conductivity and solute leakage of *Scendesmus dimorphus* cells by a factor of three (Figure 3.2), which is indicative of membrane damage. Samples at 4° C also showed an increase in electrolyte leakage (Figure 3.2), indicating that the algae was susceptible to chilling injury, similar to the effect seen in warm-season terrestrial plants.

The effect of this membrane damage on post-harvest stability and down stream processing is uncertain. Cellular damage is likely to leave algal cells less viable and therefore leave valuable cellular components more susceptible to microbial degradation when warmed. Conversely, cellular membrane disruption increases lipid extraction efficiencies. Keris-Sen et al. (2014) found that disruption of cellular membranes via ultrasound increased lipid extraction by as much as double.

Samples that had been frozen lost their ability to pellet under centrifugation, as well as loosing their gritty texture when in paste form. Differences in rheology may not affect post harvest stability, but could have significant impacts on post processing. Damaged cells may inhibit mechanical dewatering after freezing, so all mechanical dewatering should be done immediately after harvest.

Both microscopy and electrical conductivity data indicate that frozen samples have damaged or ruptured membranes, which could have effects on degradation during storage.

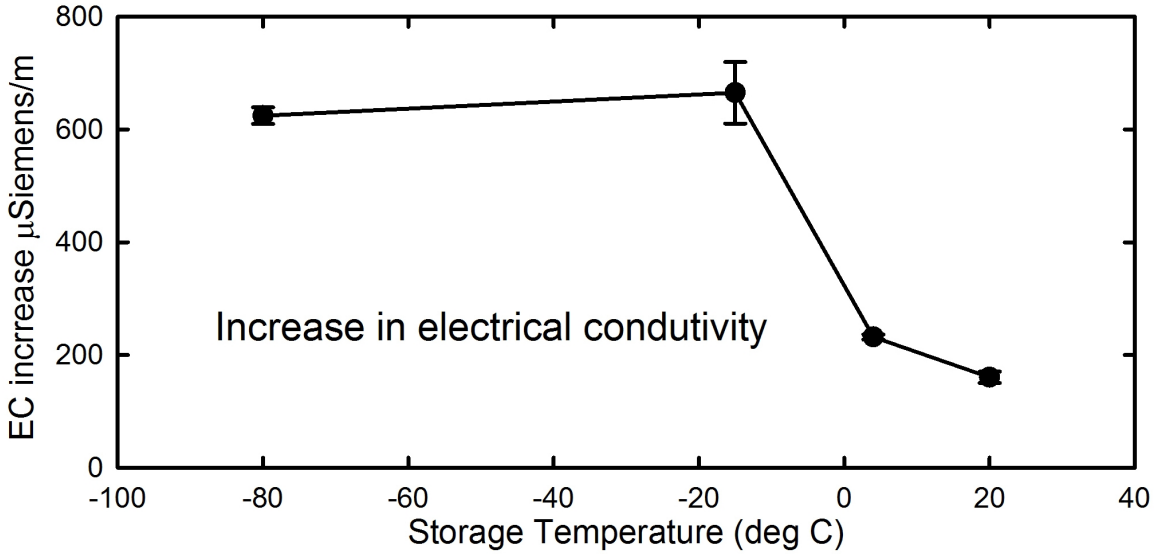

Fig. 3.2: **The effect of freezing *Scenedesmus dimorphus* on EC.** Electrical conductivity (EC) after 24 hours storage at varying temperatures, followed by a defrost period of 28 hours. The high solution EC values indicate significant membrane damage from freezing, and mild damage from chilling at 4° C.

Cellular components that are no longer protected by cell membranes may be more susceptible to degradation.

3.3 Water activity

3.3.1 Relationship of water content to water activity.

Figure 3.3 shows the relationship between water activity and water content, or moisture desorption isotherm, for *Scenedesmus dimorphus*. Though this curve may vary depending on species, post harvest processing, and growing conditions, the results will likely be similar.

A water content of 30% corresponded to a thick paste, such as seen after centrifugation. Below a water content of about 20%, or a water activity of about 0.95, the algal solution started to coagulate into either a crust if oven dried, or a powder if lyophilized. A water content of 5% or a water activity of <0.5 was considered fully dry, as drying further requires significant amounts of energy and long drying times.

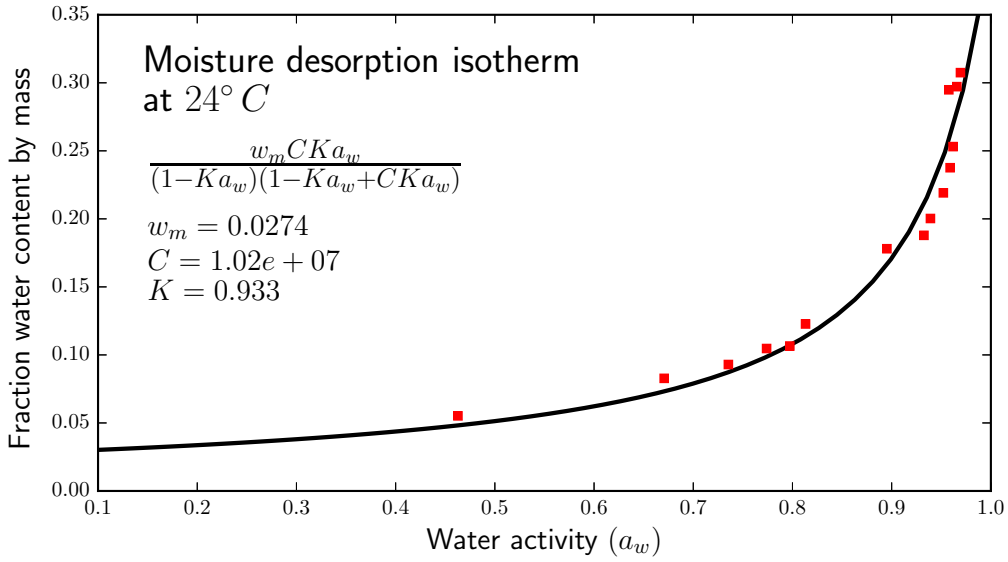

Fig. 3.3: **Moisture desorption isotherm of *Scenedesmus dimorphus*.** Isotherm is fitted to a GAB (Guggenheim, Anderson, and de Boer) equation, where w_m corresponds to the monomolecular layer and K and C are temperature dependent parameters characterizing the sorption properties of the material (Blahovec et al., 2010).

3.3.2 Effect of water activity on respiration.

After an incubation period of 24 hours, respiration decreased dramatically at a water activity of less than 0.90 (approximately 20% water content, see Fig. 3.4). This corresponds to the known water activity levels that inhibit microbial growth (Figure 1.3). At water activity levels less than 0.97, decomposition rates were less than half those found in well hydrated samples (a_w>0.98). Minimal drying was able to significantly decrease the immediate respiration rate, though much of this decrease could be contributed to the arrest of the algal cells themselves. Decomposition rates may increase over time as microbes that are more resistant to dessication begin to grow.

3.3.3 Effect of water activity on algal bioproducts

Proteins

Bulk protein was not significantly affected by water activity, with samples averaging

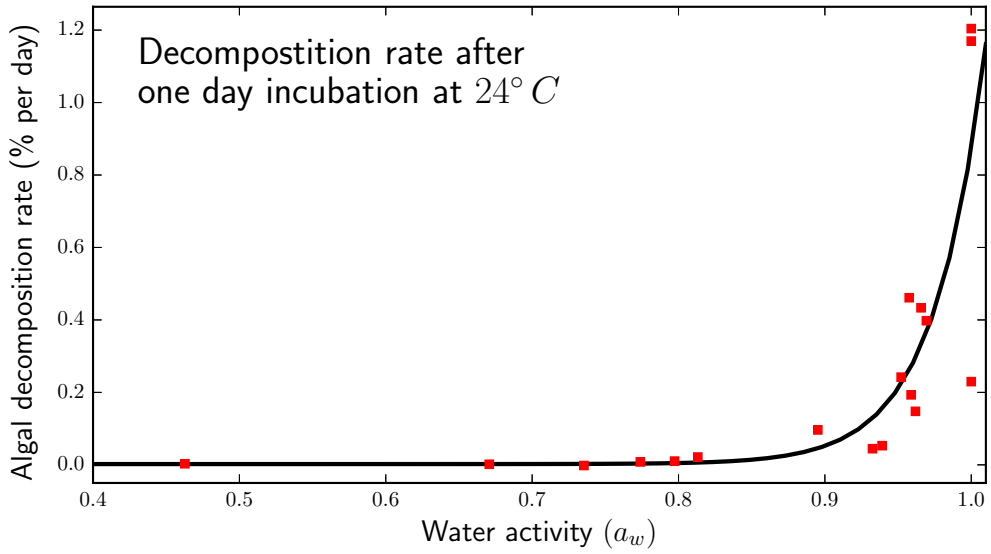

Fig. 3.4: **Algal degradation as a function of water activity.** Degradation measured as CO_2 increases in jar head space, then converted to biomass assuming degraded biomass is 60% carbon by weight. Samples were incubated for one day at 24° C.

110 ± 7 percent of original protein. The 10% average increase in protein is likely due to improvements in protein extraction techniques, specifically the cell lysing step described in section 2.10. The fact that there is no trend with water activity, and that the bulk protein levels did not decrease, indicates that bulk protein is relatively stable at room temperature regardless of water activity.

Alternatively, free amino acids increased exponentially with water activity (Fig. 3.5, FAA). Free amino acid levels increased significantly when water activity levels were greater than 0.9. The presence of free amino acids in wet samples is evidence of protease activity, as larger proteins are broken down into smaller components. The increase in free amino acid levels was fairly linear over the 30 day period (Fig. 3.6, FAA).

Lipids

Similar to proteins, FAME, which is an analog to total lipid content, was not significantly affected by water activity (Fig. 3.5, FAME) The highest FAME contents after 30 days were found in the wettest ($a_w > 0.99$) followed by the driest samples ($a_w < 0.50$). All

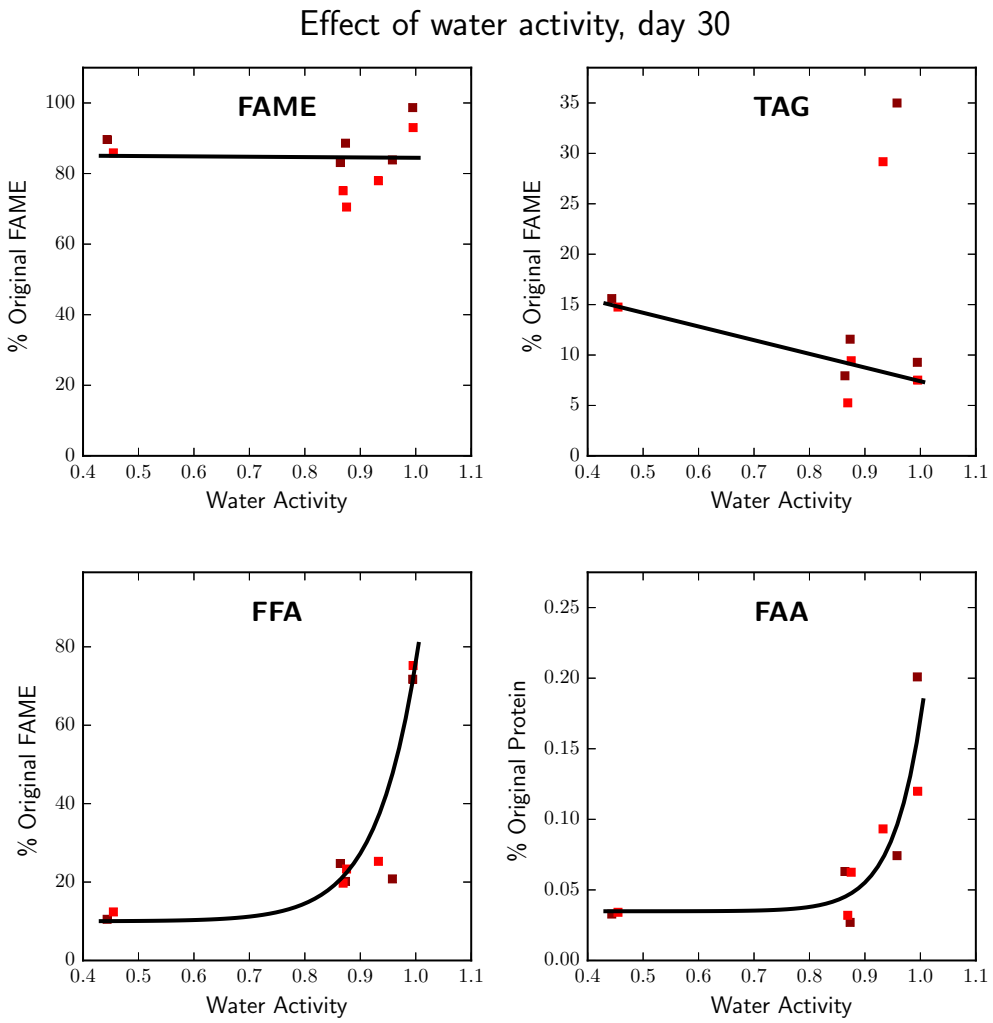

Fig. 3.5: **Effect of water activity on algal bioproduct degradation after 30 days.** Algal samples were dried as outlined in section 2.5, then incubated for 30 days at 24° C.

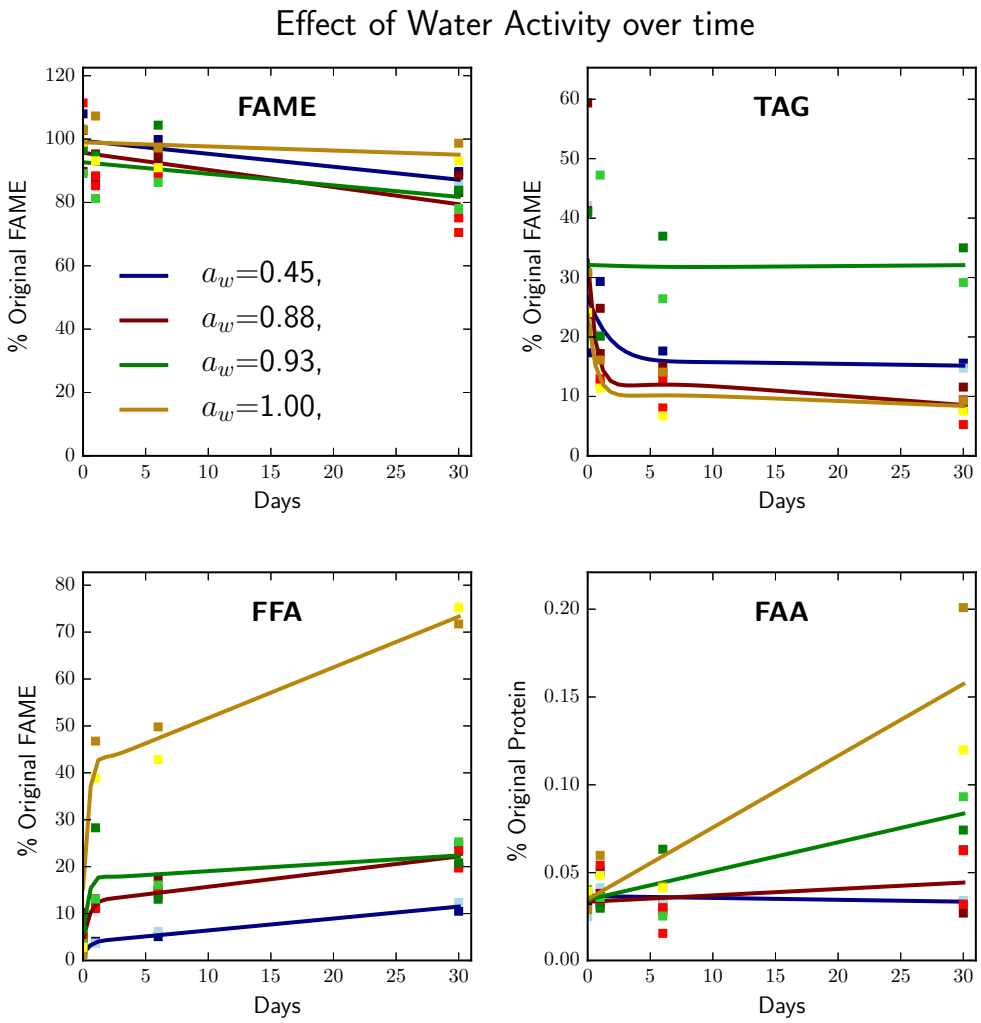

Fig. 3.6: **Algal bioproduct degradation rate over time at various water activities.** Algal samples were dried as outlined in section 2.5, then incubated for 30 days at 24° C.

samples saw a linear degradation of FAME over time, with about 15-20% lost over the 30 day incubation (Fig. 3.6). This degradation could be attributed to either degradation in to smaller molecules or volatilization.

TAG levels dropped about 60% in all samples, with the exception of those with a water activity of approximately 0.93 (Fig. 3.5, TAG). The lack of TAG degradation in the 0.93 treatment was consistent over the 30 day period, where all other treatments degraded rapidly over time (Fig. 3.6, TAG). The water activity level of 0.93 may be dry enough to inhibit hydrolysis of the triglycerides into free fatty acids, yet wet enough to inhibit autoxidation of lipids. Interestingly, the 0.93 a_w sample decrease in TAG level from initial composition is negligible, going from 8.8 to 9.0 and 13.0 to 12.0 percent of biomass for high an low nitrogen treatments respectively, yet there was still significant free fatty acid production. This would suggest that the free fatty acids were coming from non TAG sources, possibly phospholipids.

There was limited but statistically significant free fatty acid production in all cases except the most hydrated samples (Fig. 3.5, FFA). This supports the hypothesis that free fatty acids were produced at high water activity levels via hydrolysis, and less so at water activities less than 0.95. Acker (1969) showed no lipase activity at low water activity levels when a crystalline substrate was used, but saw lipase activity under the same conditions with a liquid substrate (further reviewed in Barbosa-Cánovas et al. (2008)). There was still free fatty acid production at low water activities, but less than the well hydrated samples. This indicates that lipases are not inactive, but limited either by diffusion or by a decrease in lipase functionality. As lipase is not inactive, Hydrolysis of TAG into free fatty acids may slowly continue over time.

Because there was limited reduction in FAME, high reductions of TAG, and limited production of free fatty acids at water activity levels of less than 0.9 (Fig. 3.5), the byproduct of TAG degradation did not show up as a free fatty acid, yet still shows up as FAME. This could include mono or diglycerides, or products of oxidation that are heavier weight than free fatty acids or converted back to fatty acids in the transesterification process. GC response curves from days 1 and 30 (Fig. 3.7) showed little output between the TAG and

FFA standards (between 19-31 minutes), indicating that the FAME components were not extracted with the Bligh and Dyer method.

3.4 Pasteurization

3.4.1 Effect of pasteurization on respiration

Pasteurization decreased respiration over a one day period (Fig. 3.8), however, after 100 hours of incubation at 24° C, the respiration rate of the pasteurized samples exceeded that of the control. This suggests that the pasteurization process killed both bacterial and algal cells, diminishing the initial respiration rate, but the resulting nutrient rich slurry was an ideal environment for microbial organisms. The respiration rate of the control is likely attributed to the living algal cells themselves, as it follows a linear patten indicating respiration without growth, whereas the pasteurized sample follows an exponential pattern indicating microbial growth.

3.4.2 Effect of pasteurization on algal bioproducts

Proteins

Protein degradation was highest during long pasteurization times (Fig. 3.10, Pro), with a 40% reduction in total protein when pasteurized for 30 min at 65° C. Free amino acids were also reduced by pasteurization (Figs. 3.9 and 3.10, FAA). This suggests that both protein and free amino acids were degraded into non-amino compounds, likely products of Maillard reactions. The products of Maillard reactions are generally indigestible by humans. Based on our findings, algal proteins are more resistant to high heats than to long heating times, so rapid heating and cooling may be beneficial if using this method to preserve proteins.

Lipids

FAME degradation was relatively unaffected by pasteurization temperatures (Fig. 3.9, FAME), though there was slightly increased degradation at higher temperatures, with about

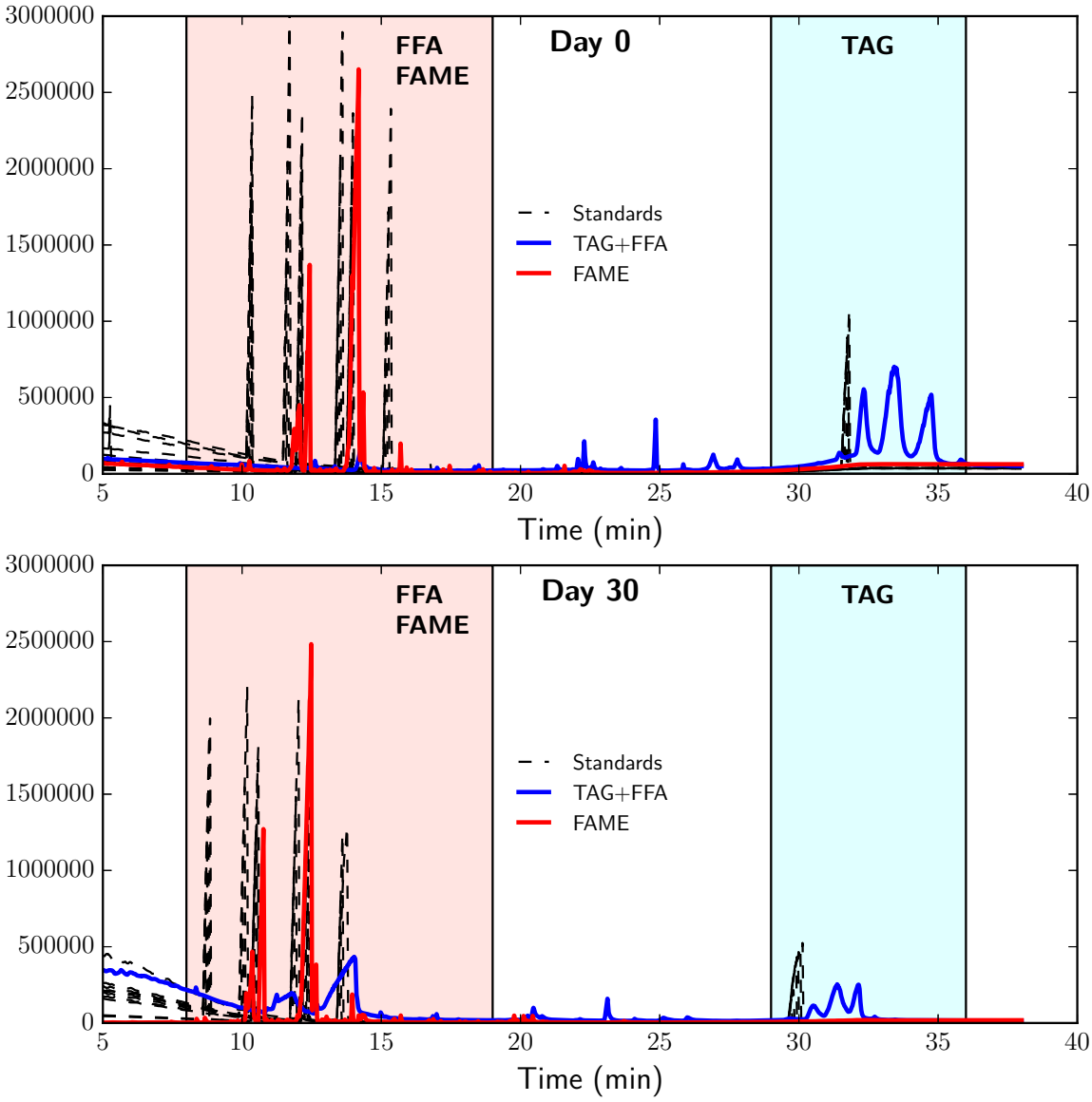

Fig. 3.7: **Sample GC response.** GC response curves from days 0 and 30.

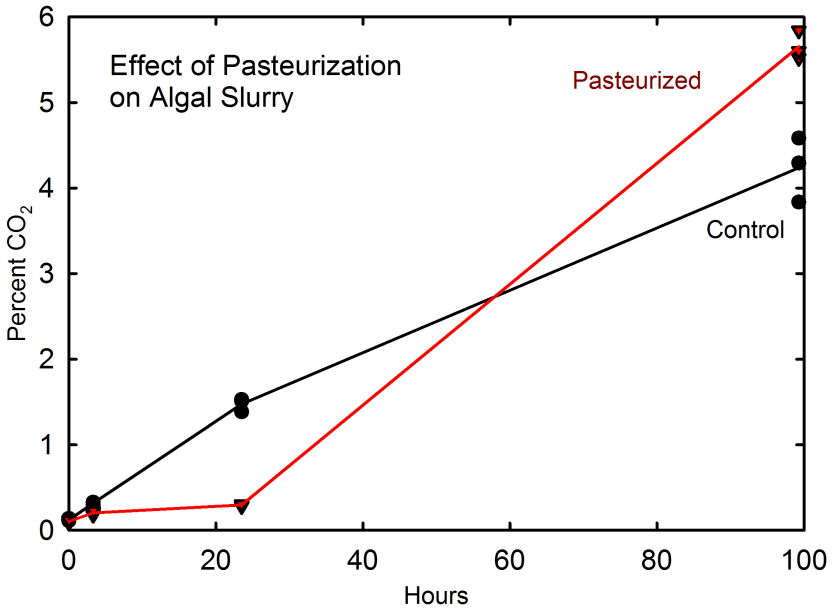

Fig. 3.8: **The evolution of CO_2 after pasteurization of algal slurry samples (10% solids).** Samples were pasteurized at 66° Cfor 30 minutes. The pasteurized samples had significantly reduced respiration after 24 hours, but surpassed the control after 100 hours.

10% degradation at the highest temperatures (90° C). Similarly, TAG degradation was highest at high temperatures, though all treatments had average reductions of 20 to 50%. Free fatty acids were also degraded by high temperatures, with all treatments at about 50% degradation.

The product of TAG degradation is unclear, as TAG and free fatty acids were degraded without a reduction in FAME. These could be products of oxidation that are heavier weight than the free fatty acids, or compounds that are converted to methyl esters in the transesterification process. This may indicate a decrease in nutritional quality. As no free fatty acids were produced, pasteurization may not have an effect of palatability, depending of the product of TAG degradation. It is unclear how this would impact biofuel performance.

3.5 Hot air drying

3.5.1 Effect of hot air drying on algal bioproducts

Figure 3.11 shows a representative sample temperature during the drying process. The

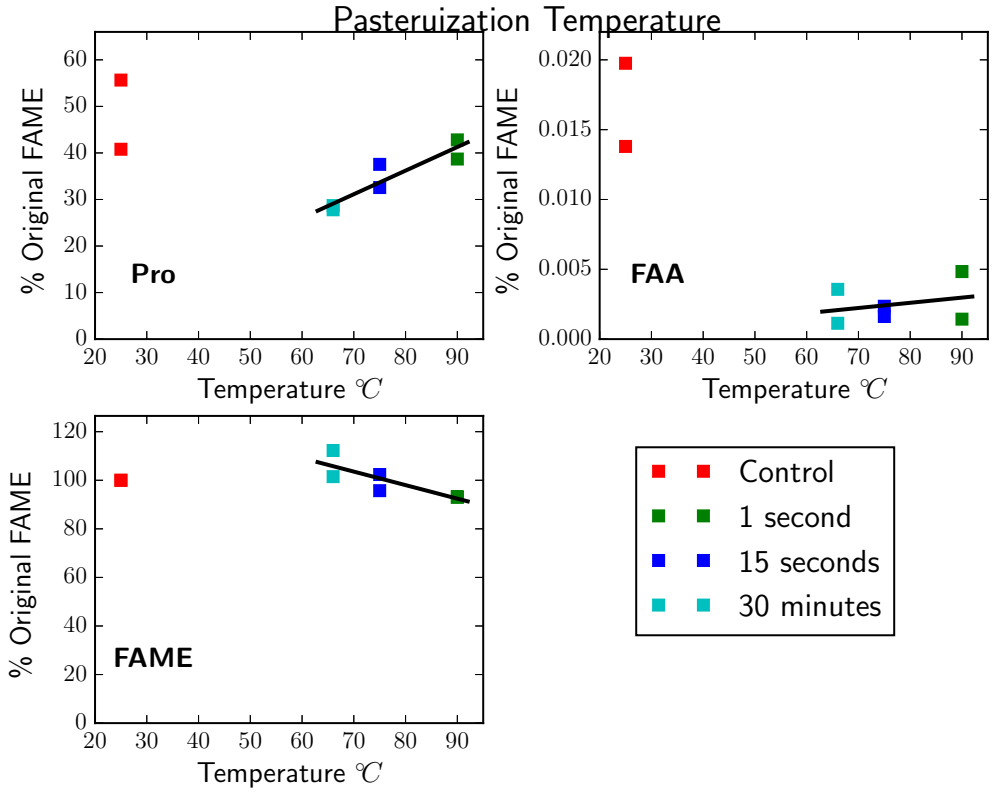

Fig. 3.9: **Effect of pasteurization temperature on degradation of bioproducts.**

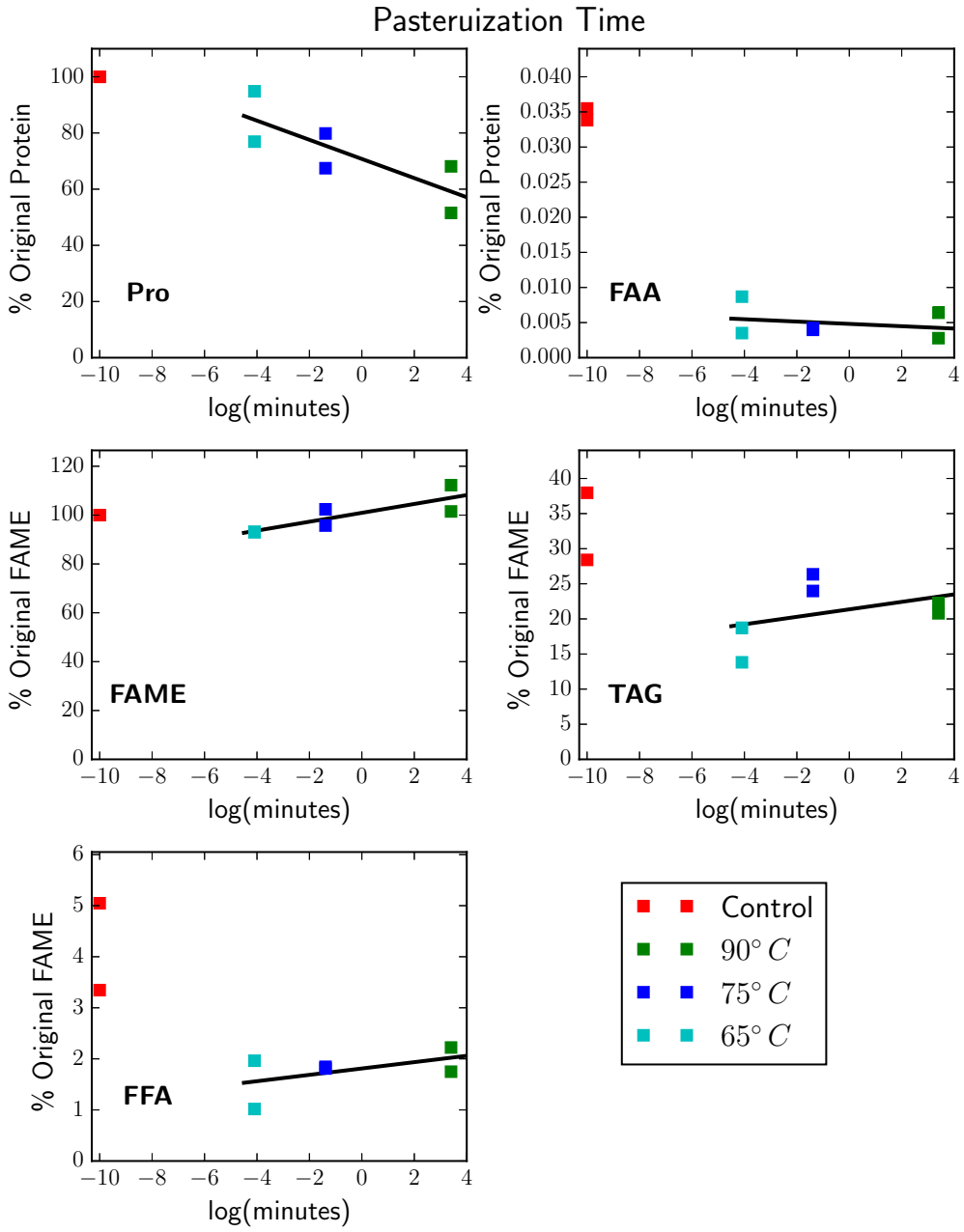

Fig. 3.10: **Effect of pasteurization time on degradation of bioproducts.**

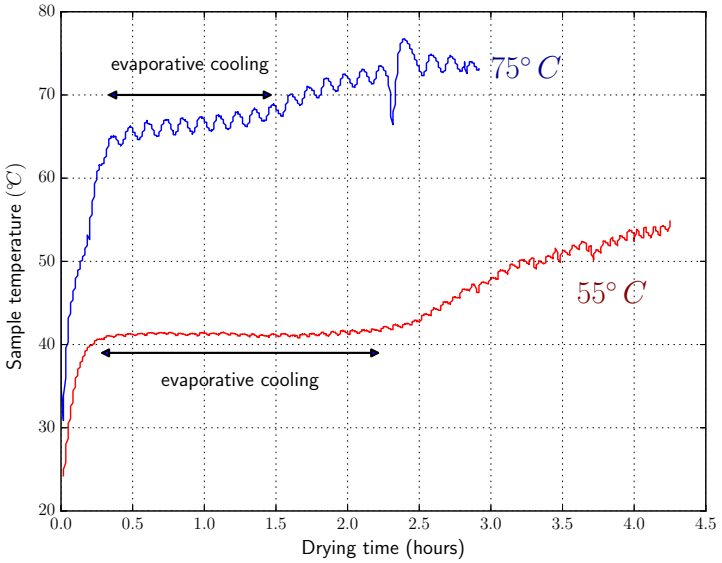

Fig. 3.11: **Sample temperature during hot air drying.** Samples were dried to an average water activity of 0.86. Data is from replicate samples with thermocouples inserted during drying. These replicates were only used to measure temperatures during drying not analyzed further.

55° C oven samples maintained about 42° C for the majority of the drying time, compared to >65° C in the 75° C oven samples. The sample temperature was maintained lower than the surrounding temperature by convective cooling, significantly cooler in the 55° C drying oven. Drying time increased by about 9% in the 55° C drying oven.

Proteins

Total protein degraded more over long drying times (>3 hours) with lower temperatures (Figs. 3.12 and 3.13, Pro). Protein levels were shown to increase under the high temperature drying treatment (75° C). This effect is not likely real, but an artifact of increased cell digestibility and therefore increased signal when quantified. We can assume that since the 55° C treatment decreased in protein content, that there was real degradation, though the actual amount cannot be accurately quantified from this data. Free amino acid levels were unaffected by heat drying indicating no protease activity in either treatment.

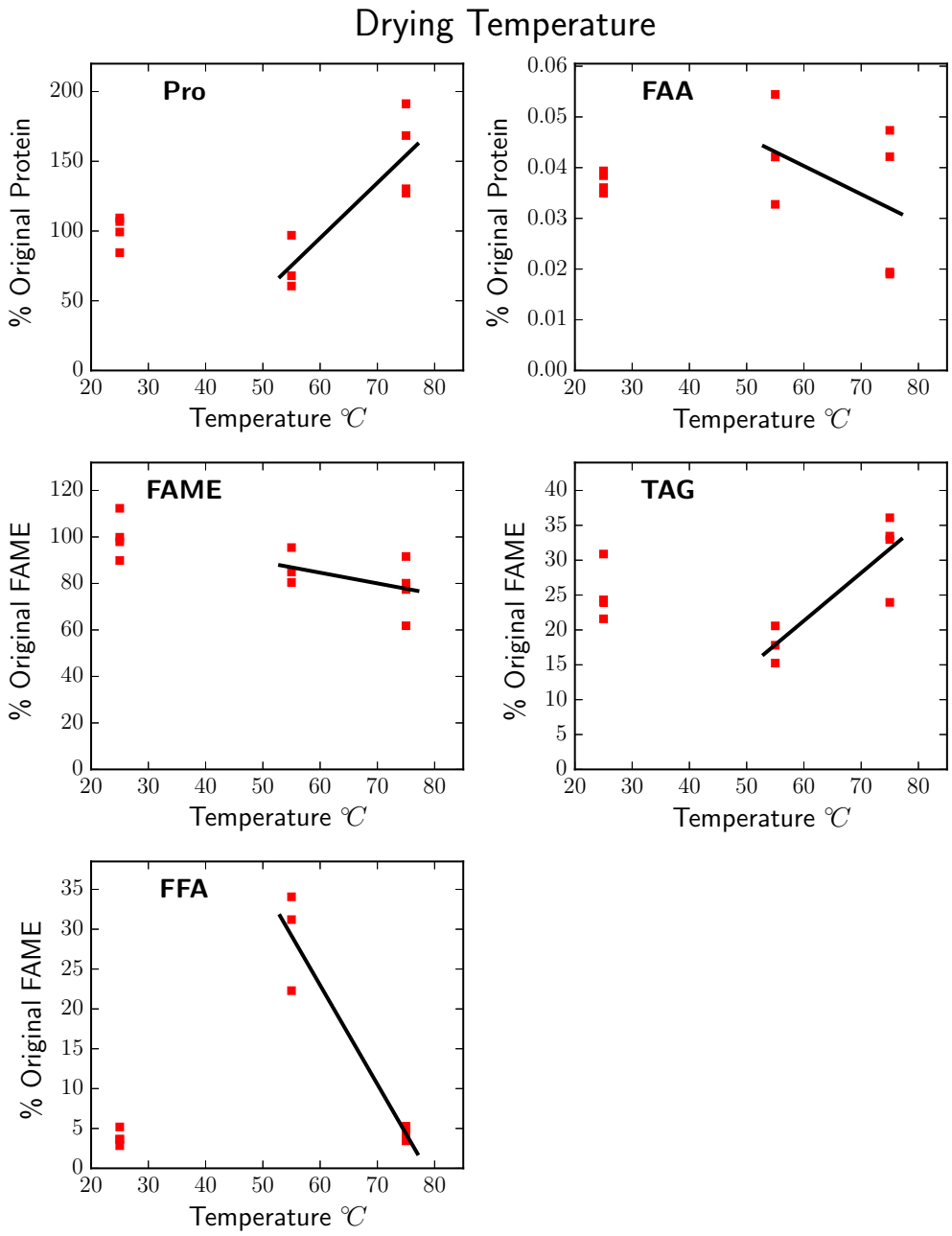

Fig. 3.12: **Algal bioproduct degradation as a function of drying oven air temperature.** Samples were dried to an average water activity of 0.86.

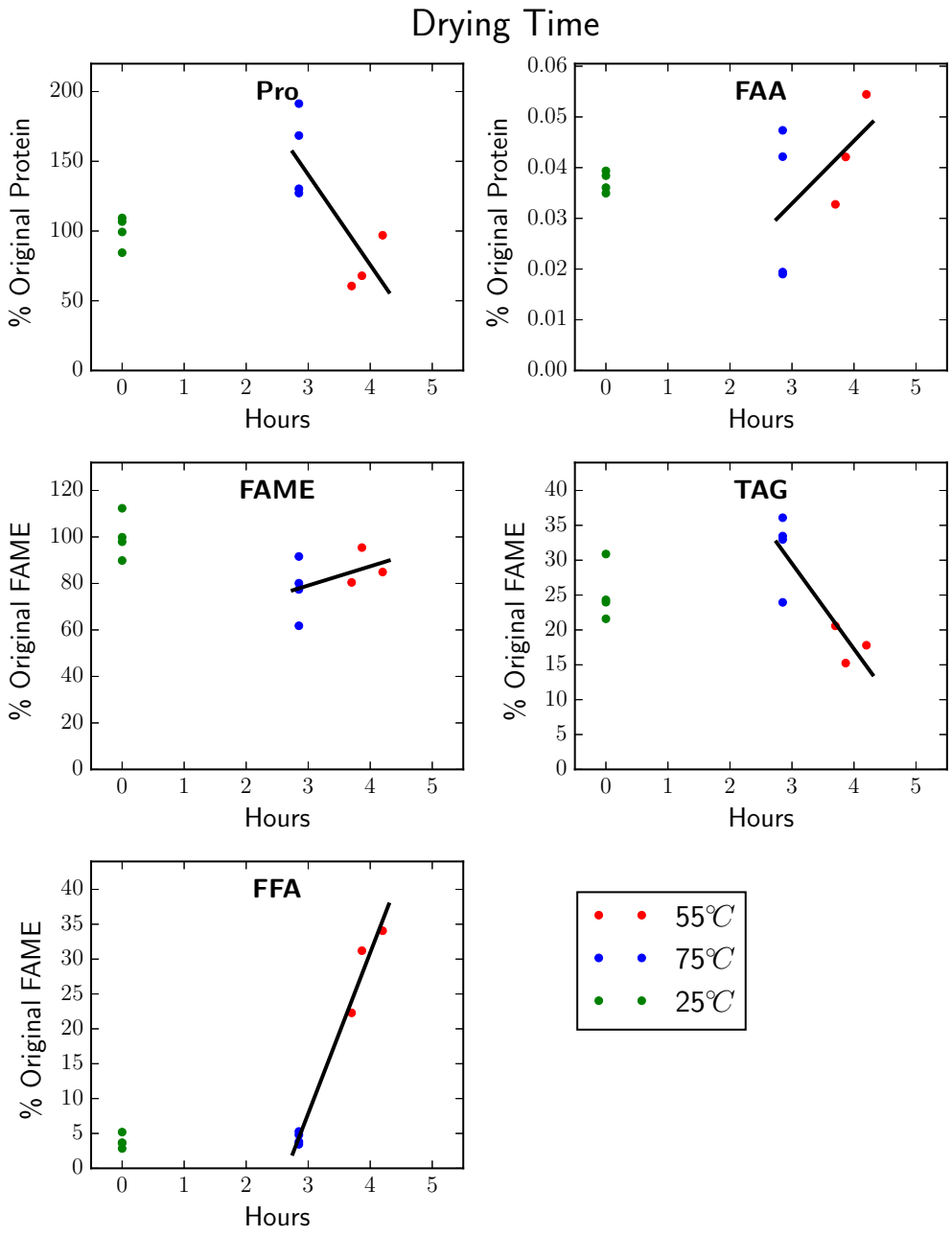

Fig. 3.13: **Algal bioproduct degradation rate after drying for different time periods.** Samples were dried to an average water activity of 0.86.

Lipids

FAME degraded under all drying treatments, with about 20% and 18% lost when dried at temperatures of 75° C and 55° C respectively. TAG degradation and free fatty acid production were both highest in the 55° C treatments. Free fatty acid was produced twice as much as TAG was degraded, suggesting that some of the free fatty acids came from sources other than TAG, such as membrane phospholipids.

3.6 Deactivation of lipase

Though both pasteurization and hot air drying showed some degradation of TAG, only hot air drying at 55° C showed an increase in free fatty acid levels (Figs. 3.9 and 3.12). As seen in Figure 3.11, sample temperatures while drying at an air temperature of 55° C stayed at about 42° C for over 2 hours. Compared to the 75° C air temperature samples, sample temperatures rapidly increased to about 60° C, and then rose slowly for the remainder of the drying time. As sample temperatures in the 75° C air drying and the 65° C pasteurization treatments were subject to heating for 1 or more hours with little free fatty acid production, it is likely that these sample temperatures inactivated lipase enzymes, whereas the 42° C sample temperatures did not. These algal lipases are likely deactivated at temperatures between 42 and 60° C.

The dry conditions of hot air drying may have protected lipase enzymes, which cleave TAG molecules into free fatty acids. Turner et al. (1995) found the denaturation temperature of liver carboxylesterase increased as a function of decreasing water activity, by as much as 50° C in anhydrous conditions. The low water contents are thought to prevent enzymes from being able to unfold, thus deactivating them (Troller and Christian, 1978). Time may also be a factor, as pasteurization samples were processes relatively quickly then frozen, whereas the hot air dried samples were subject to drying temperatures for 2.5 to 4.5 hours. The fact that the 60° C pasteurization treatment also had minimal free fatty acid levels, while still being heated for 60 minutes give credence to the lipase degradation hypothesis.

TAG decreases and FFA increases were never precisely coupled. In the case of the 0.93 a_w treatments seen in Figure 3.5, almost no TAG was found to degrade, yet FFA

levels doubled. Similarly, while TAG content in the 55° C drying oven samples dropped by 62 and 32 mg per gram biomass for high and low nitrogen, respectively, FFA content increased by 80 and 106 mg per gram biomass for high and low nitrogen, respectively. These differences would indicate that the free fatty acids are coming from an alternative source, with the next largest pool being membrane phospholipids. It is unclear why the lipase would preferentially target membrane lipids. This effect could also be an experimental artifact, though the mechanism of which is unclear.

3.7 Composition of non-FFA producing TAG degridation

The degradation of TAG without the production of free fatty acids was prevalent in both pasteurized and low water activity samples. Both these scenarios saw either no or limited reductions of FAME content. This is likely the product of oxidation. It is clear that the reduction in TAG is would result in a decrease in nutritional value, but as the FAME content is minimally degraded, it is unclear how this would affect biofuel production. If the products are a result of oxidation, the resulting fuel would likely have a lower energy density, making it a less desirable fuel.

Chapter 4

Conclusions

4.1 Freezing and chilling

While freezing is likely the best option for preserving valuable compounds, it is also energy intensive and expensive. The resulting product is not the same as freshly harvested algae after freezing and/or chilling. This has implications for research, where membrane degradation may affect processing. Previously frozen samples that are used for lipid extractions may give different results when compared to unfrozen samples. Statements of whether the algae have been previously frozen should be standard when reporting results of post harvest processes such as dewatering techniques, bioproduct extractions, or storage. Chilling may be a viable compromise to limit cellular degradation, because it can preserve samples and minimize membrane damage.

4.2 Protein as a nutritional product

As protein degradation rates were low even with relatively high water activities, simple mechanical dewatering may suffice when harvesting crude proteins, as least for moderate storage times (1 month). This applies only to crude protein content, as it is unknown from this research the effect on protein quality and bioavailability. Low value uses, such as livestock feed, could benefit from the cost reductions of limited processing, where quantity is not the primary concern, though the current high costs of algal production may make this an inviable option when compared to traditional crops.

If the end product is intended for human consumption, the degradation of triglycerides to free fatty acids may make algal protein unpalatable even with low lipid contents. Therefor, these higher value scenarios would benefit from some sort of post processing, such as pasteurization. All pasteurization temperatures prevented free fatty acid production, as well

as decreased free fatty acid levels, so simple heat treatments during the harvesting phase could produce a relatively stable, palatable food product. Heating may even increase the bioavailability of the protein. Pasteurization for protein preservation would require the optimization of time and temperature, as long pasteurization times decreased total protein content.

4.3 Lipids

Algal lipid production would benefit from post production methods to denature lipase activities. Moderate heat increases were shown to inhibit free fatty acid production. This could have major implications for the algae industry, as drying has been a major hurdle in both making the process net energy positive and profitable. The results indicate that drying is not the most effective means of preserving the lipids, and TAG may be best preserved by storing as a moderate water activity and drying immediately before extraction. If the triglycerides can be stabilized from lipase degradation, less energy intensive methods for drying, such as solar or low temperature drying, could be utilized. Also, minimal post processing could result in a relatively stable product, allowing for storage and transport before extraction. If pasteurization is incorporated into the harvesting step, wet extraction methods could be utilized without interactions of FFA. Though pasteurization decreased free fatty acid levels, it also decreased TAG levels, so optimizing time and temperatures for lipase deactivation with minimal lipid degradation would be critical.

4.4 Energy and cost of lipase deactivation

Using the specific heat of water (4.19 $^{kJ}/_{kg^{\circ}C}$), and assuming a 10% algal slurry and a 50° C change in temperature for pasteurization (from 25° C to 75° C), we can approximate that 2.1 megajoules of energy is needed to pasteurize one kilogram of algae. Further, using the 2014 U.S. national average industrial price for natural gas ($^{\$0.20}/_{m^3}$, U.S. Energy Information Agency), and assuming 35 megajoules per cubic meter of natural gas, we can estimate that the cost would be on the order of $0.01 per kg algae, which is a small fraction of the production costs.

4.5 Further research

Direct measurement of lipase activity and degraded lipid volatiles would greatly support the hypothesis laid out here. As the results presented here focused on loss of desired products, understanding of the specific degradation pathways would allow for more precise prevention of degradation. Also, measurements of protein digestibility and nutrient quality over time would give further insight into how stable protein really is.

4.6 Final remarks

Postharvest degradation is a key component to the viable production of algal bioproducts, yet has been understudied thus far. Algae decomposition is primarily a result of degradation of products by the microbe harvested rather than by microbes that would opportunistically colonize and spoil. Because of this, deactivation of algal enzymes may help overcome some of the obstacles of algaculture harvesting and processing. These results are an initial step in characterizing a stable algal product and there is ample room to extend on these findings.

References

Acker, L.W., 1969. Water activity and enzyme activity. Food Technology 23, 1257–&.

Adams, C., Godfrey, V., Wahlen, B., Seefeldt, L., Bugbee, B., 2013. Understanding precision nitrogen stress to optimize the growth and lipid content tradeoff in oleaginous green microalgae. Bioresource Technology 131, 188–194.

Barbosa-Cánovas, G.V., Fontana Jr, A.J., Schmidt, S.J., Labuza, T.P., 2008. Water activity in foods: fundamentals and applications. volume 13. John Wiley & Sons.

Becker, E., 2007. Micro-algae as a source of protein. Biotechnology Advances 25, 207–210.

Becker, W., 2004. 18 Microalgae in Human and Animal Nutrition. Handbook of microalgal culture: biotechnology and applied phycology , 312.

Blahovec, J., Yanniotis, S., others, 2010. GAB generalised equation as a basis for sorption spectral analysis. Czech Journal Food Sciences 28, 345–354.

Bold, H.C., 1942. The cultivation of algae. The Botanical Review 8, 69–138.

Borowitzka, M.A., 1997. Microalgae for aquaculture: opportunities and constraints. Journal of Applied Phycology 9, 393–401.

Borowitzka, M.A., Moheimani, N.R., 2013. Algae for Biofuels and Energy. volume 5. Springer.

Brennan, L., Owende, P., 2010. Biofuels from microalgae—A review of technologies for production, processing, and extractions of biofuels and co-products. Renewable and Sustainable Energy Reviews 14, 557–577.

Brown, M., Jeffrey, S., Volkman, J., Dunstan, G., 1997. Nutritional properties of microalgae for mariculture. Aquaculture 151, 315–331.

Campbell, J.E., Lobell, D.B., Genova, R.C., Field, C.B., 2008. The Global Potential of Bioenergy on Abandoned Agriculture Lands. Environ. Sci. Technol. 42, 5791–5794.

Chen, L., Liu, T., Zhang, W., Chen, X., Wang, J., 2012. Biodiesel production from algae oil high in free fatty acids by two-step catalytic conversion. Bioresource Technology 111, 208–214.

Chisti, Y., 2007. Biodiesel from microalgae. Biotechnology advances 25, 294–306.

Clarens, A.F., Resurreccion, E.P., White, M.A., Colosi, L.M., 2010. Environmental Life Cycle Comparison of Algae to Other Bioenergy Feedstocks. Environ. Sci. Technol. 44, 1813–1819.

Clayton, J.R., Dortch, Q., Thoresen, S.S., Ahmed, S., 1988. Evaluation of methods for the separation and analysis of proteins and free amino acids in phytoplankton samples. Journal of Plankton Research 10, 341–358.

Cordero, B., Voltolina, D., 1997. Viability of mass algal cultures preserved by freezing and freeze-drying. Aquacultural Engineering 16, 205–211.

Field, C.B., Behrenfeld, M.J., Randerson, J.T., Falkowski, P., 1998. Primary production of the biosphere: integrating terrestrial and oceanic components. Science 281, 237–240.

Field, C.B., Campbell, J.E., Lobell, D.B., 2008. Biomass energy: the scale of the potential resource. Trends in Ecology & Evolution 23, 65–72.

Fitzherbert, E.B., Struebig, M.J., Morel, A., Danielsen, F., Brühl, C.A., Donald, P.F., Phalan, B., 2008. How will oil palm expansion affect biodiversity? Trends in Ecology & Evolution 23, 538–545.

Hooijer, A., Page, S., Canadell, J.G., Silvius, M., Kwadijk, J., Wösten, H., Jauhiainen, J., 2010. Current and future CO2 emissions from drained peatlands in Southeast Asia. Biogeosciences 7, 1505–1514.

Karlsson, J.O., Toner, M., 1996. Long-term storage of tissues by cryopreservation: critical issues. Biomaterials 17, 243–256.

Keris-Sen, U.D., Sen, U., Soydemir, G., Gurol, M.D., 2014. An investigation of ultrasound effect on microalgal cell integrity and lipid extraction efficiency. Bioresource Technology 152, 407–413.

Milledge, J.J., Heaven, S., 2012. A review of the harvesting of micro-algae for biofuel production. Reviews in Environmental Science and Bio/Technology 12, 165–178.

Molina Grima, E., Belarbi, E.H., Acién Fernández, F.G., Robles Medina, A., Chisti, Y., 2003. Recovery of microalgal biomass and metabolites: process options and economics. Biotechnology advances 20, 491–515.

Pienkos, P.T., Darzins, A., 2009. The promise and challenges of microalgal-derived biofuels. Biofuels, Bioproducts and Biorefining 3, 431–440.

Pittman, J.K., Dean, A.P., Osundeko, O., 2011. The potential of sustainable algal biofuel production using wastewater resources. Bioresource Technology 102, 17–25.

Quinn, J.C., Catton, K.B., Johnson, S., Bradley, T.H., 2013. Geographical assessment of microalgae biofuels potential incorporating resource availability. Bioenergy Research 6, 591–600.

Quinn, J.C., Yates, T., Douglas, N., Weyer, K., Butler, J., Bradley, T.H., Lammers, P.J., 2012. Nannochloropsis production metrics in a scalable outdoor photobioreactor for commercial applications. Bioresource Technology 117, 164–171.

Ramadhas, A., Jayaraj, S., Muraleedharan, C., 2005. Biodiesel production from high FFA rubber seed oil. Fuel 84, 335–340.

Rodolfi, L., Zittelli, G.C., Bassi, N., Padovani, G., Biondi, N., Bonini, G., Tredici, M.R., 2009. Microalgae for Oil: Strain Selection, Induction of Lipid Synthesis and Outdoor Mass Cultivation in a Low-Cost Photobioreactor. Biotechnology and Bioengineering 102, 100–112.

Sharma, K.K., Garg, S., Li, Y., Malekizadeh, A., Schenk, P.M., 2013. Critical analysis of current microalgae dewatering techniques. Biofuels 4, 397–407.

Show, K.Y., Lee, D.J., Chang, J.S., 2013. Algal biomass dehydration. Bioresource Technology 135, 720–729.

Thomsen, M.K., Lauridsen, L., Skibsted, L.H., Risbo, J., 2005. Temperature Effect on Lactose Crystallization, Maillard Reactions, and Lipid Oxidation in Whole Milk Powder. J. Agric. Food Chem. 53, 7082–7090.

Troller, J., 2012. Water activity and food. Elsevier.

Troller, J.A., Christian, J., 1978. 3 - Enzyme Reactions and Nonenzymatic Browning, in: Christian, J. (Ed.), Water Activity and Food. Academic Press, pp. 48–68.

Turner, N.A., Duchateau, D.B., Vulfson, E.N., 1995. Effect of hydration on thermostability. Biotechnology letters 17, 371–376.

Uduman, N., Qi, Y., Danquah, M.K., Forde, G.M., Hoadley, A., 2010. Dewatering of microalgal cultures: A major bottleneck to algae-based fuels. Journal of Renewable and Sustainable Energy 2, 012701.

Vyas, A.P., Verma, J.L., Subrahmanyam, N., 2010. A review on FAME production processes. Fuel 89, 1–9.

Wahlen, B.D., Morgan, M.R., McCurdy, A.T., Willis, R.M., Morgan, M.D., Dye, D.J., Bugbee, B., Wood, B.D., Seefeldt, L.C., 2013. Biodiesel from Microalgae, Yeast, and Bacteria: Engine Performance and Exhaust Emissions. Energy & Fuels 27, 220–228.

Wahlen, B.D., Willis, R.M., Seefeldt, L.C., 2011. Biodiesel production by simultaneous extraction and conversion of total lipids from microalgae, cyanobacteria, and wild mixed-cultures. Bioresource Technology 102, 2724–2730.

Wehtje, E., Adlercreutz, P., 1997. Water activity and substrate concentration effects on lipase activity. Biotechnology and Bioengineering 55, 798–806.

Xu, L., (Wim) Brilman, D.W., Withag, J.A., Brem, G., Kersten, S., 2011. Assessment of a dry and a wet route for the production of biofuels from microalgae: Energy balance analysis. Bioresource Technology 102, 5113–5122.

Appendices

Appendix A

Economic Analysis of Greenhouse Lighting: Light Emitting Diodes vs. High Intensity Discharge Fixtures

Abstract. Lighting technologies for plant growth are improving rapidly, providing numerous options for supplemental lighting in greenhouses. Here we report the photosynthetic (400-700 nm) photon efficiency and photon distribution pattern of two double-ended HPS fixtures, five mogul-base HPS fixtures, ten LED fixtures, three ceramic metal halide fixtures, and two fluorescent fixtures. The two most efficient LED and the two most efficient double-ended HPS fixtures had nearly identical efficiencies at 1.66 to 1.70 micromoles per joule. These four fixtures represent a dramatic improvement over the 1.02 micromoles per joule efficiency of the mogul-base HPS fixtures that are in common use. The best ceramic metal halide and fluorescent fixtures had efficiencies of 1.46 and 0.95 micromoles per joule, respectively. We also calculated the initial capital cost of fixtures per photon delivered and determined that LED fixtures cost five to ten times more than HPS fixtures. The five-year electric plus fixture cost per mole of photons is thus 2.3 times higher for LED fixtures, due to high capital costs. Compared to electric costs, our analysis indicates that the long-term maintenance costs are small for both technologies. If widely spaced benches are a necessary part of a production system, the unique ability of LED fixtures to efficiently focus photons on specific areas can be used to improve the photon capture by plant canopies. Our analysis demonstrates, however, that the cost per photon delivered is higher in these systems, regardless of fixture category. The lowest lighting system costs are realized when an efficient fixture is coupled with effective canopy photon capture.

A.1 Introduction

Rapid advances in lighting technology and fixture efficiency provide an expanding number of options for supplemental lighting in greenhouses, including numerous LED fixtures (light emitting diode, see Bourget (2008); Morrow (2008) for a history of LED lighting in horticulture). Significant improvements have been made in all three high intensity discharge (HID, which includes high pressure sodium, HPS, and ceramic metal halide, CMH) fixture components: the lamp (often referred to as the bulb), the luminaire (often referred to as the reflector) and the ballast. High pressure sodium fixtures with electronic ballasts and double-ended lamps are now 1.7 times more efficient than older mogul-base HPS fixtures.

Lighting technologies vary widely in how radiation is distributed (Fig. A.1). There is no ideal pattern of radiation distribution for every application. In large greenhouses with small aisles and uniformly spaced plants, the broad, even output pattern typically emitted from HPS fixtures provides uniform (little variation over a large area) light distribution and increased capture of photosynthetic photons. In smaller greenhouses with spaced benches, the more focused pattern typically found in LED fixtures can maximize radiation transfer to plant leaves. As the area (height of width) covered by plants increases, the need for more focused radiation decreases (Fig. A.2).

In greenhouse applications, selection among lighting options should primarily be made based on the cost to deliver photons to the plant canopy surface. This analysis includes two parameters: 1) the fundamental fixture efficiency, measured as micromoles of photosynthetic photons per joule of energy input, and 2) the canopy photosynthetic (400-700 nm) photon flux (PPF) capture efficiency, which is the fraction of photons transferred to the plant leaves.

Electrical efficiency for plant growth

The electrical efficiency of lamps is often expressed using units for human light perception (efficacy; lumens or foot-candles out per watt in) or energy efficiency (radiant watts out per electrical watt in). Photosynthesis and plant growth, however, is determined by moles of photons. It is thus important to compare lighting efficiency based on photon efficiency, with units of micromoles of photosynthetic photons per joule of energy input. This is especially important with LEDs where the most electrically efficient colors are in the deep

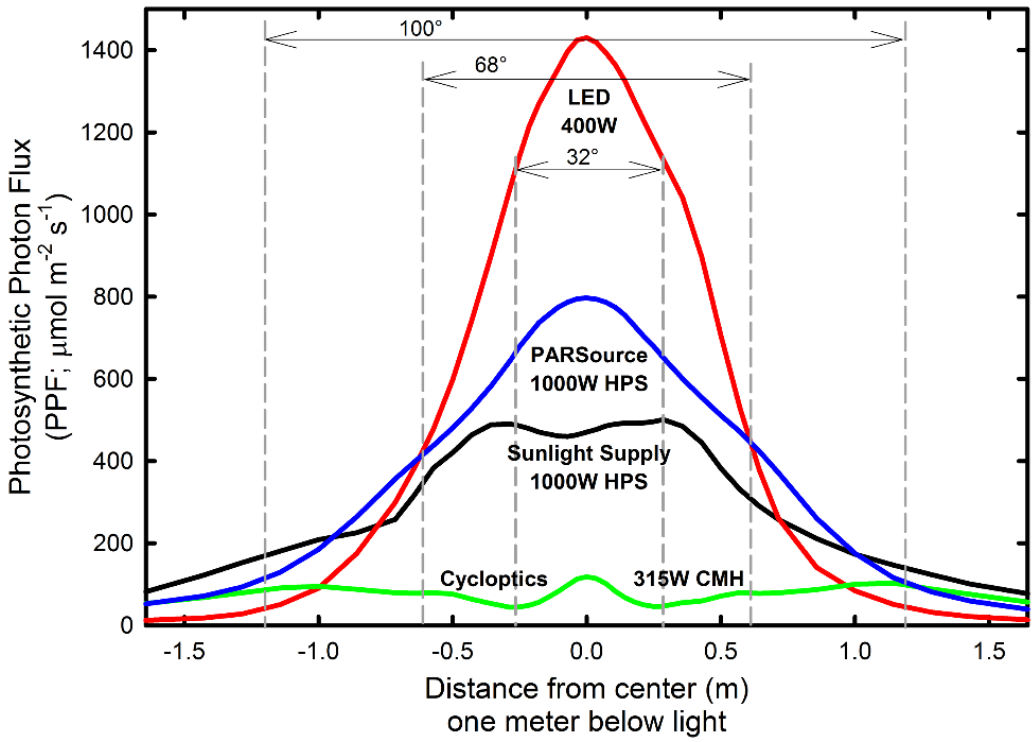

Fig. A.1: **The photon distribution of four fixtures with similar photon efficiency.** Each line represents a cross section of the photon intensity below the fixture. The LED fixture (Lighting Sciences Group) uses optics to achieve a narrow distribution, with the majority of the photons falling in a concentrated pattern directly below the fixture. Conversely, the Cycloptics ceramic metal halide fixture is designed for even light distribution, and therefore casts uniform radiation over a large surface area. Since the area increases exponentially as the distance from the center increases, an equal photon flux farther from the center represents a larger quantity of total photons.

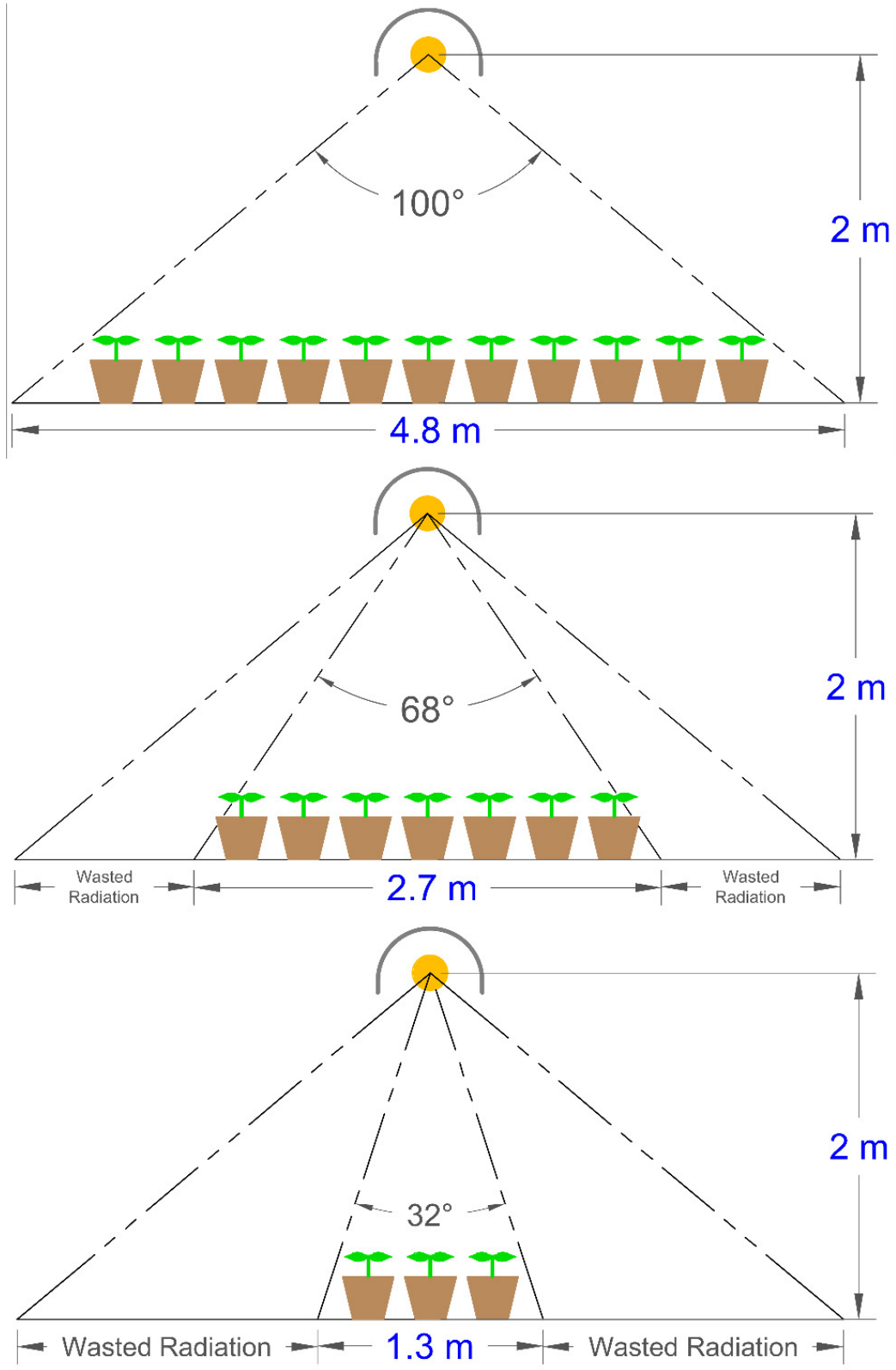

Fig. A.2: **Canopy photon capture efficiency.** As the plant growth area under the fixture gets smaller, wasted radiation often increases. This figure illustrates the concept of canopy photon capture efficiency. Two meters was chosen as a typical mounting height, but this can be scaled as a unit-less ratio. Multiple overlapping fixtures are typically used to minimize PPF variation over a large area.

Table A.1: **Efficiency of individual LEDs at a drive current of 700 mA.**

LED Color	Peak wavelength or color temperature	Photon efficience $\mu mol/J$	Electrical efficiency (%)	Luminous efficiency lm/W
Cool white	5650 Kelvin	1.52	33	111
Red	655 nm	1.72	32	47
Blue	455 nm	1.87	49	17

red and blue wavelengths. A dramatic example of this is the comparison of red, blue, and cool white LEDs (Table A.1). The lower radiant energy content of red photons allows more photons to be delivered per unit of input energy (radiant energy is inversely proportional to wavelength, PlanckâĂŹs Equation). Conversely, blue LEDs can have a 53% higher energy efficiency (49% vs. 32%) but only a 9% higher photon efficiency (1.87 vs. 1.72).

Effect of light quality

There is considerable misunderstanding over the effect of light quality on plant growth. Many manufacturers claim significantly increased plant growth due to light quality (spectral distribution or the ratio of the colors). A widely used estimate of the effect of light quality on photosynthesis comes from the Yield Photon Flux (YPF) curve, which indicates that orange and red photons between 600 to 630 nm can result in 20 to 30% more photosynthesis than blue or cyan photons between 400 and 540 nm (Fig. A.3)(Inada, 1976; McCree, 1972). When light quality is analyzed based on the YPF curve, HPS lamps are equal to or better than the best LED fixtures because they have a high photon output near 600 nm and a low output of blue, cyan, and green light (Nelson and Bugbee, 2013).

The YPF curve, however, was developed from short-term measurements made on single leaves in low light. Over the past 30 years, numerous longer-term studies with whole plants in higher light indicate that light quality has a much smaller effect on plant growth rate than light quantity (Cope et al., 2014; Johkan et al., 2012). Light quality, especially the fraction of blue light, has been shown to alter cell expansion rate, leaf expansion rate (Dougher and Bugbee, 2004), plant height and plant shape in several species (Cope and Bugbee, 2013;

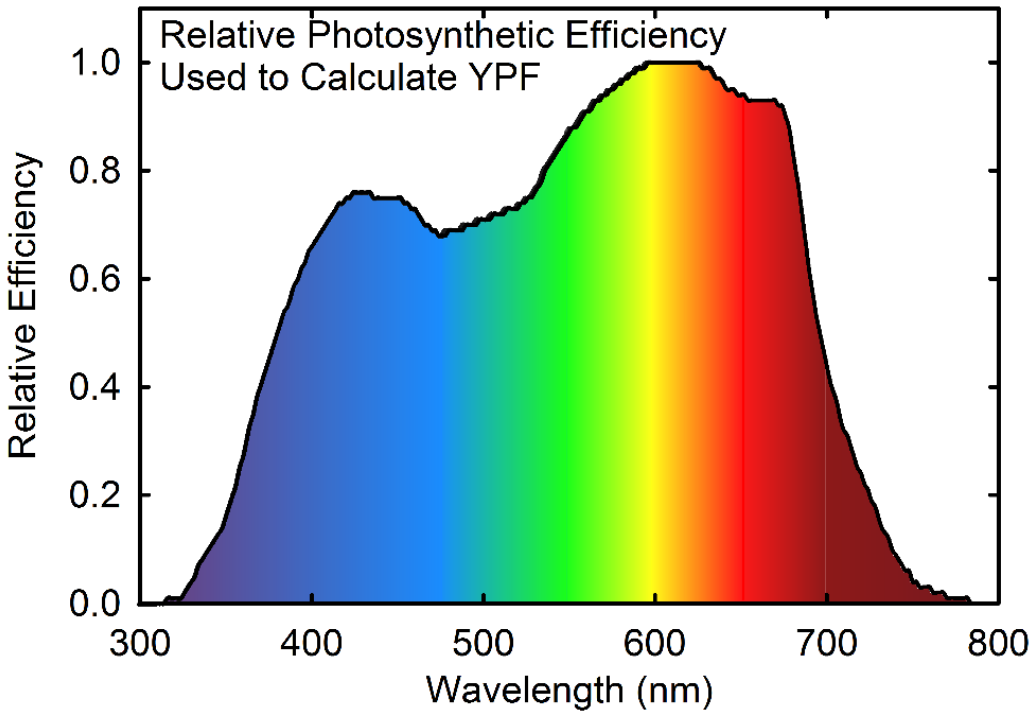

Fig. A.3: **Yield photon flux curve.** Effect of wavelength on relative photosynthesis per incident photon for a single leaf in low light (less than 150 $^{\mu mol}/_{m^2 s}$) (McCree, 1972).

Dougher and Bugbee, 2001; Yorio et al., 2001), but it has only a small direct effect on photosynthesis. The effects of light quality on fresh or dry mass in whole plants typically occur under low or no sunlight conditions, and are caused by changes in leaf expansion and radiation capture during early growth (Cope et al., 2014).

Unique aspects of LED fixtures.

The most electrically efficient colors of LEDs, based on moles of photosynthetic photons per joule, are blue, red, and cool white, respectively (Fig. A.4), so LED fixtures generally come in combinations of these colors. LEDs of other colors can be used to dose specific wavelengths of light to control aspects of plant growth (Yang et al., 2012), due to their monochromatic nature (see Massa et al. (2008) for a review of unique LED applications). Ultraviolet (UV) radiation is typically absent in LED fixtures because UV LEDs significantly reduce fixture efficiency. Sunlight has 9% UV (percent of PPF), and standard electric lights have 0.3 to 8% UV radiation (percent of PPF) (Nelson and Bugbee, 2013). A lack of UV

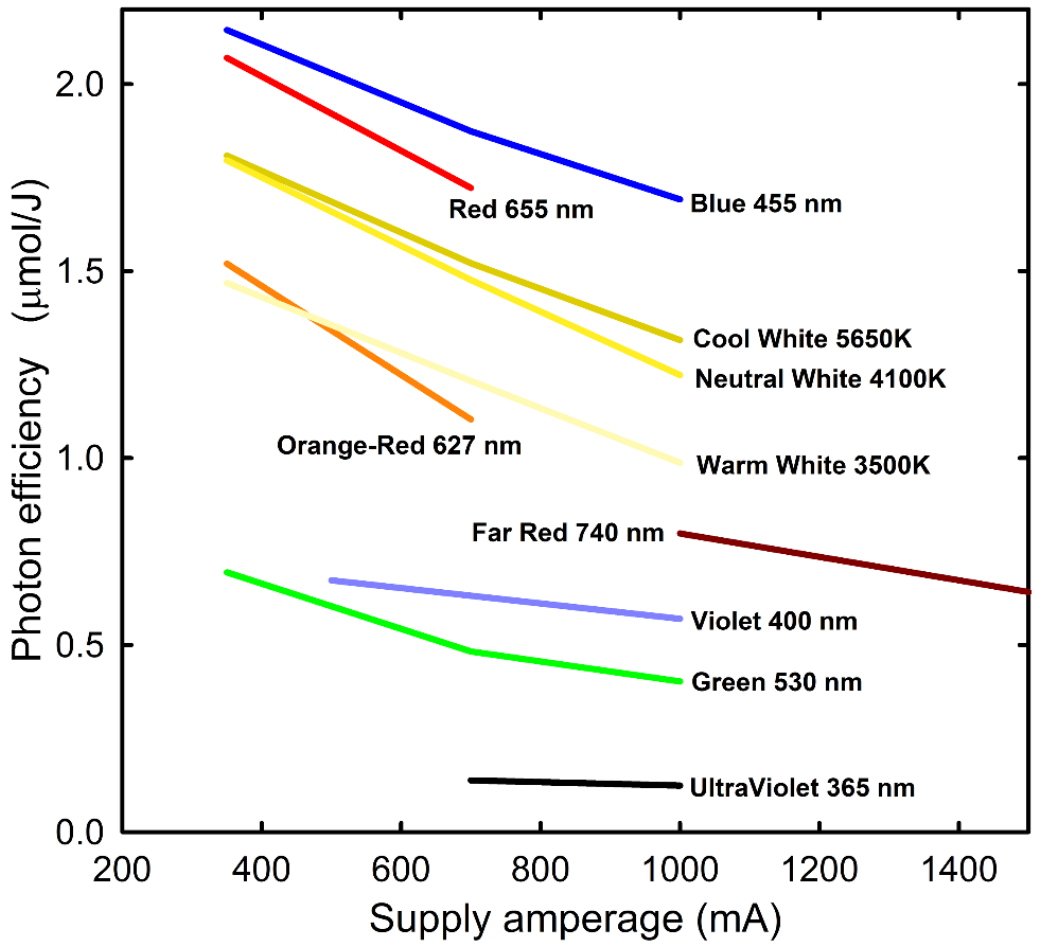

Fig. A.4: **Effect of drive amperage and color on photon efficiency of LEDs.** Data for Philips Lumileds LEDs (May 2014), courtesy of Mike Bourget, Orbitec.

causes disorders in some plant species (e.g. Intumescence; (Morrow and Tibbitts, 1988)) and this is a concern with LED fixtures when used without sunlight. LED fixtures for supplemental photosynthetic lighting also have minimal far-red radiation (710 to 740 nm), which decreases the time to flowering in several photoperiodic species (Craig and Runkle, 2013). Green light (530 to 580 nm) is low or absent in most LED fixtures and these wavelengths better penetrate through the canopy and are more effectively transmitted to lower plant leaves (Kim et al., 2004). The lack of UV, green, and far-red wavelengths, however, should be minimal when LEDs are used in greenhouses, because most of the radiation comes from broad spectrum sunlight.

Our objective is to help growers and researchers select the most cost effective fixture options for supplemental lighting in greenhouses. To achieve this goal we measured two fundamental components of each fixture: 1) the efficiency of conversion of electricity to photosynthetic photons that are delivered to a horizontal surface below the lamp, and 2) the distribution pattern of these photons below the fixture

A.2 Materials and Methods

Fixture efficiency.

Measurements of fixture efficiency (lamp, luminaire, and ballast) were made by integrating sphere and flat-plane integration techniques. The integrating sphere measurements were made by a certified testing laboratory (TÃIJV SÃIJD America) that specializes in the measurement of the efficiency of lighting fixtures using the IES LM79-08 measurement standard (, 2008). Radiometric output was converted to photon output at each nanometer interval using PlankâĂŹs Equation and then integrated from 400 to 700 nanometers. The radiation measurements were calibrated to NIST reference standards. These measurements of fixture efficiency are considered repeatable to within 1 %.

Flat plane integration.

Measurements were made in a dark room with flat black walls using a quantum sensor (LI-COR model LI-190, Lincoln, NE, USA), that was calibrated for each fixture with an NIST-traceable calibrated spectroradiometer (model PS-200, Apogee Instruments, Logan, UT, USA). This calibration is necessary to correct for small spectral errors (Âś3 %) in the quantum sensor that occur because of imperfect matching of the ideal quantum response (Blonquist and Bugbee, 2013). Measurements were made in three radial, straight lines below a level fixture and spatially integrated over a flat plane below the fixture to determine total photon output. Measurements were made 2.5 cm apart near the center, increasing to 10 cm near the perimeter as PPF variation decreased (121 measurements total). Fixtures were mounted 0.7 meters above the surface and measurements were made up to a 1.5 meter

radius from the center and extrapolated to infinity using an exponential decay function. Fixture height is optional, depending on the size of the room and measurement area as long as measurement resolution captures the spatial variation in fixture output. The flat-plane integration measurements were used to quantify the pattern of photon distribution from the fixture. Total fixture output from these measurements was similar to measurements made using an integrating sphere (Table A.2). When redundant measurements were available, the integrating sphere measurements were used to quantify fixture efficiency. Power draw and electrical characteristics were measured using a multimeter and a current clamp (Fluke model 289, Everett, WA, USA).

Cost of electricity.

In the United States, commercial electric rates vary widely by region, ranging from $0.07 in Idaho to $0.17 in New York, with residential rates averaging $0.02 higher, and industrial rates $0.02 lower. Electric rates in Europe, and many other countries, can be more than double the rates in the United States. As electricity becomes more expensive, improved lighting becomes more valuable. See U.S. Energy Information Administration for a summary of current electric rates by state and region (accessed April 2014). We used a discounted cash flow model assuming a 5% per year cost of capital on future electrical costs.

A.3 Results

The photon efficiency (micromoles per joule) and cost per mole of photons for four categories of lighting technologies (HPS, LED, ceramic metal halide, and fluorescent), in 22 fixtures, are shown in Table A.3. One fixture of each model was tested. This table also shows the five-year electric plus fixture costs per mole of photons. Most fixtures (lamp, luminaire and ballast) are now more efficient than the common 1000-W magnetic-ballast, mogul-base HPS fixtures (i.e. Sunlight Supply, 1.02 Âţmol per joule). If photons coming out of the fixture at all downward angles are considered (180Âř), the capital cost of the most efficient 400-W LED fixtures we tested is five to seven times more per photon than the 1000-W, double-ended, electronic ballast HPS fixtures (Gavita, ePapillion, Table A.3).

The high capital cost of LEDs makes the five year cost per mole of photons more than twice that of HPS fixtures (Table A.3 and Fig. A.5A).

Table A.3 assumes that all of the photons emitted from the fixture are absorbed by plant leaves. In Table A.4, the area under the fixture in which the photons are considered captured by plants is progressively reduced, and the cost per mole of photons increases as more photons are lost around the perimeter. When only highly focused radiation is considered useful (34°), some LED fixtures have a lower cost per photon than the best HPS fixtures (Table A.4, Fig. A.1, Fig. A.5B and Fig. A.6), but because photons are lost around the perimeter at this narrow angle, the cost per photon absorbed by plants is much greater. The lowest cost per photon is realized when a large canopy can be arranged to capture the photons.

A.4 Discussion

Importance of photon capture.

As reviewed in the introduction, lighting system efficiency is the combined effect of efficient fixtures and efficient canopy photon capture efficiency. Precision luminaires, lenses (e.g. model vivid white, Lighting Sciences Group inc.), or adjustable angle LEDs (e.g. model SPYDR 600, BML inc.) can be used to apply highly focused lighting specifically to the plant growth areas. This is valuable in small greenhouses with widely spaced benches. Canopy photon capture efficiency can be maximized, to above 90%, for large greenhouses with narrow aisles regardless of fixture type. The use of LED intracanopy lighting can increase capture rates to near 100%, and may have other beneficial effects such as increased light sharing with intracanopy leaves (Gómez et al., 2013; Both et al., 2000). The concentration of heat from HID fixtures makes intracanopy lighting infeasible with high wattage HPS fixtures. Just as precision irrigation can improve water efficiency, precision lighting can improve electrical efficiency.

Effect of fixture shadow.

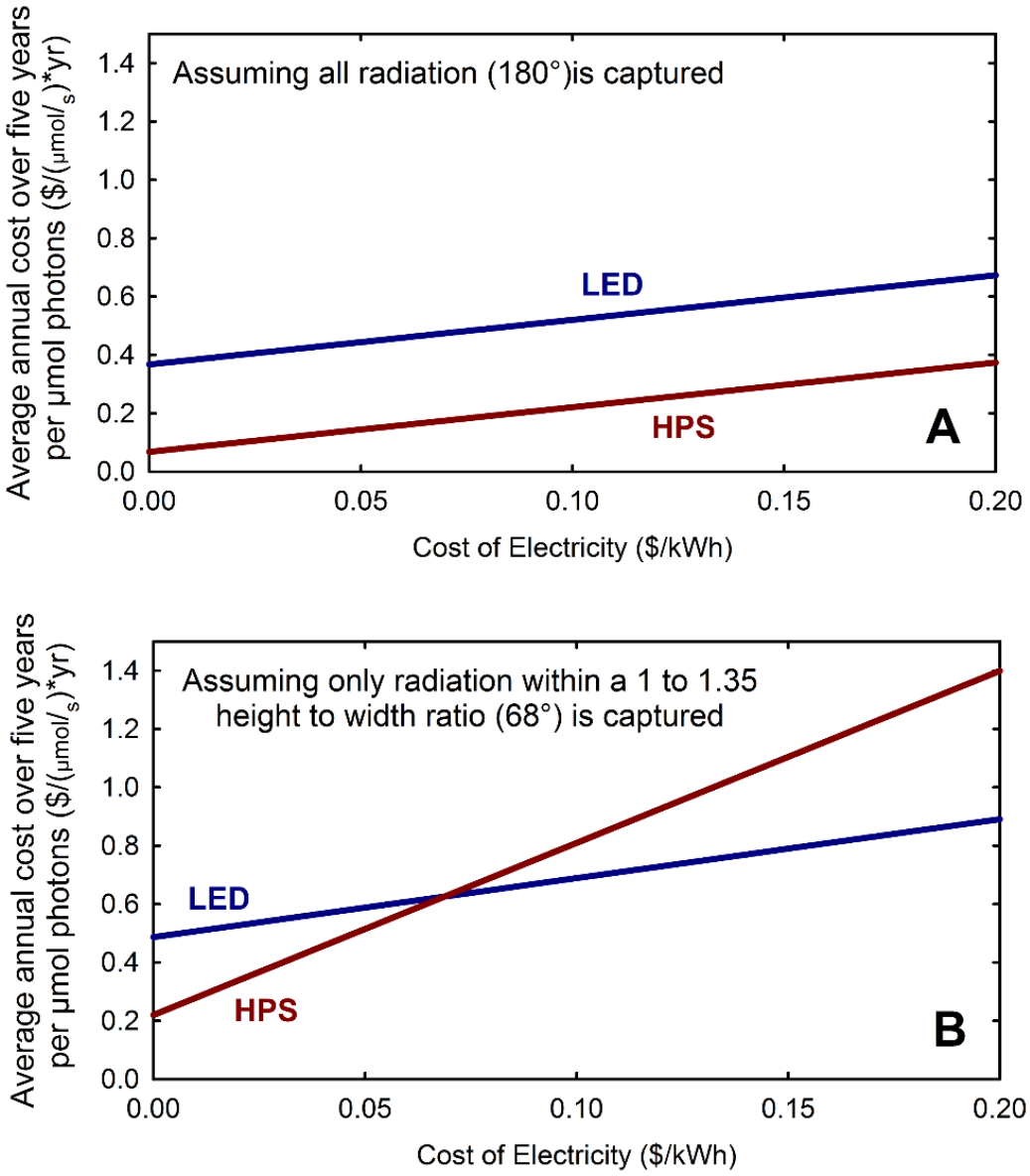

Fig. A.5: **Effect of electricity price on average annual cost over five years for two capture scenarios.** (A) When all radiation is assumed captured, the most efficient HPS fixture (Gavita) has a lower average annual five-year cost per photon than the most efficient LED fixture (Red/Blue fixture, Lighting Sciences Group). (B) When only a narrow region below the fixture (68°) is considered to be captured (e.g. on benches), the LEDs can have a lower cost per photon then HPS fixtures, but the cost per photon increases for both fixtures.

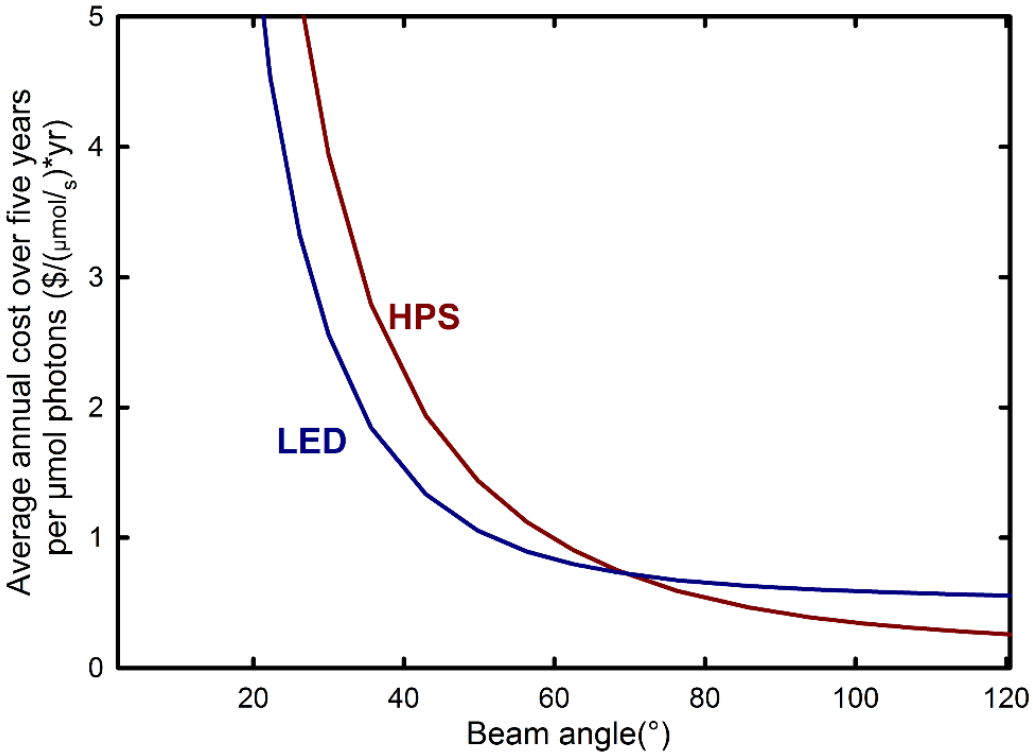

Fig. A.6: **Effect of canopy capture efficiency on average annual cost over five years.** The cost per mole of photons for LEDs (Red/Blue LED from Lighting Sciences Group) becomes more favorable than the best HPS fixtures (Gavita) when the lighting area is less than 68°from center, assuming $0.11 per kWh cost of electricity and 3000 hours per year use (approximate cumulative operation time at latitudes from 40 to 50 degrees).

All fixtures block radiation from the sun, and the shadow is proportional to the size of the fixture. For the same photon output, 400-W HPS, ceramic metal halide, fluorescent, and LED fixtures block significantly more sunlight than 1000-W HPS fixtures. We did not include the effect of the shadow in this analysis, but this effect significantly favors the more energy dense, higher wattage HPS fixtures. In the long-term, LEDs can take advantage of innovative design options like mounting along greenhouse support structures, which could provide light without extra shading. Longer, narrower LED fixtures may be preferable to rectangular fixtures because the duration of the shadow is shorter. Fluorescent fixtures, including induction fluorescent, have large shadows relative to their photon output (and have low photon efficiencies) and are therefore generally not economical for greenhouse lighting.

Installation, annual maintenance costs, and life expectancy.

Installation costs include wiring for fixtures and physically hanging the fixture In our experience, the cost of installation is similar for both fixture types, although installation costs can be reduced by fewer, higher wattage fixtures. The annual maintenance costs are small relative to the cost of the electricity, and these costs are better established for HPS fixtures than for LED fixtures.Maintenance costs are largely determined by the life expectancy of the fixture.

Double-ended HPS lamps (1000-W) have a life expectancy of 10,000 hours to 90% survival (based on manufacturer literature), or 3.3 years when used an average of 8 hours per day or 3,000 hours per year (traditional mogul-base lamps have industry reported life expectancies of 10,000 to 17,000 hours, to 90% survival, and cost approximately $40). The cost of a 1000-W, double-ended replacement lamp is about $140, which averages to $28 per year if we assume a lamp will be replaced once in the first five years. This lamp replacement cost can increase to $30 to $35 per year when the labor to replace the bulb is included, but this is a small amount compared to the approximately $600 per year annual electric cost to operate the fixture. Adding the cost of lamp replacement increases the five-year cost of operation by approximately 5%.

When operated at favorable temperatures, individual LEDs generally have a predicted

lifetime (to 70% of the initial light output) of up to 50,000 hours, about 16.7 years when used an average 8 hours per day or 3000 hours per year. The economic life for LED fixtures for plant lighting has not been established, but it depends on the value of the product being produced. The high capital cost of replacement means that LED fixtures would be operated longer, in spite of diminished photon output. Replacement of individual LEDs is more expensive than replacing an HID lamp. The life expectancy of LEDs is reduced if they are driven by higher amperage to achieve a higher output, or exposed to high temperatures. Fixtures may be warmed by radiation from sunlight. The cooler the LED temperature, the longer they last. Power supplies, fans, and other components in LED fixtures can fail well before the LEDs themselves. Fan failure would increase LED temperature and may not be immediately noticed by the user. These components are replaceable, but the labor costs to change fixture components increases operating costs.

For these reasons we have not included a differential operating cost between LED and HPS fixtures. We assumed that maintenance costs will be minimal during the first five years for all types of fixtures. Electronic ballasts for 1000-W HPS lamps are still a relatively new technology, and fixtures vary in quality. We have experienced premature failures of LED power supplies, LED circuit boards, HPS lamps, and electronic HPS ballasts in our greenhouse operations. LED fixtures with improved power supplies and optimized operating amperages are available from reputable manufacturers. Improvements in these new technologies are occurring rapidly.

Importance of PPF uniformity.

PPF uniformity is critical in many greenhouse applications, especially in floriculture. It is easier to achieve uniformity with fixtures that have broad distribution of photons. Economically, the value of uniform plants may outweigh the cost of wasted photons. Uniformity has been well characterized and modeled with HID lights (Both et al., 2000; Ferentinos and Albright, 2005), but these techniques have not yet been rigorously applied to LED fixtures. Ciolkosz et al. (2001) showed that uniform light on the perimeter of a greenhouse requires higher fixture densities in the outer rows, and consequentially may increase the amount of

radiation lost beyond the edge of the growing area, decreasing canopy photon capture. HPS fixtures with narrower focus luminaires tend to have lower photon efficiencies.

Effect of fixture efficiency on heating and cooling costs.

Improved electrical efficiency reduces the cooling load in a greenhouse, which increases the value of efficient fixtures when cooling is required. The best HPS and LED fixtures have nearly identical efficiency, so cooling costs are similar for both fixture categories. The ability to cycle LED fixtures, which prematurely ages other fixture types, could be used to stabilize the heating and cooling load in a greenhouse during partly cloudy days, which could improve temperature control and increase the lifetime of cooling system equipment.

Additional thermal radiation is useful in warming the plant canopy during the heating season, but is detrimental if the canopy is too warm. When sunlight supplies adequate PPF, supplemental lighting is usually turned off.

A.5 Conclusions.

The most efficient HPS and LED fixtures have equal efficiencies, but the initial capital cost per photon delivered from LED fixtures is five to ten times higher than HPS fixtures. The high capital cost means that the five-year cost of LED fixtures is more than double that of HPS fixtures. If widely spaced benches are a necessary part of a production system, LED fixtures can provide precision delivery of photons and our data indicate that they can be a more cost effective option for supplemental greenhouse lighting.

Manufacturers are working to improve all types of lighting technologies and the cost per photon will likely continue to decrease as new technologies, reduced prices, and improved reliability become available.

Table A.2: **Efficiency of fixtures using integrating sphere measurements compared with flat-plane integration.**

	TUV SÜD America integrating sphere			USU flat plane integration			flat plane / integrating sphere
Fixture	Elec. input (W or J/S)	Photon output ($\mu mol/s$)	Photon efficiency ($\mu mol/J$)	Elec. input (W or J/S)	Photon output ($\mu mol/s$)	Photon efficiency ($\mu mol/J$)	$\frac{\mu mol/J}{\mu mol/J}$
Gavita Pro 1000DE	1033	1751	1.70	1041	1814	1.74	2.7%
ePapillion 1000W	1041	1767	1.70	1037	1937	1.87	9.1%
LSG violet	384	653	1.70	391	628	1.61	-6.0%
SPYDR 600	326	541	1.66	332	575	1.73	4.4%
LSG red/white	390	634	1.63	397	601	1.51	-7.5%
Illumitex NeoSol	279	390	1.40	281	386	1.38	-1.8%
ParSource GLXII	1026	1334	1.30	1008	1433	1.42	8.6%
Lumigrow Pro 325	304	390	1.29	304	355	1.17	-10.1%
California Lightworks solarstorm	337	350	1.04	343	331	0.96	-7.7%
Black Dog BD360U	339	339	1.00	346	323	0.93	-7.2%
Apache AT120WR	169	163	0.96	167	150	0.90	-7.2%
iGrow 400W	394	374	0.95	397	354	0.89	-6.5%
Lumigrow es330	318	284	0.90	317	270	0.85	-5.1%
Hydrogrow Sol 9	423	378	0.89	430	396	0.92	2.9%

Table A.3: **Photon efficiency and cost per mole of photons, assuming all photons (180°) are captured by plants.**

Lamp type and Ballast	Fixture producer	Electric input ($^{J}/_{s}$ or watts)	Photon output ($^{\mu mol}/_{s}$)	Photon efficiency ($^{\mu mol}/_{J}$)	Cost of one fixture ($)	Fixtures needed per $^{millimol}/_{J}$	Fixture cost per mol/s $/$ $^{\mu mol}/_{s}$	Electric cost per Âţmol photons $^{\$}/_{^{mol}/_{s}\,yr}$	Five year electric cost per Âţmol photons $^{\$}/_{^{mol}/_{s}\,yr}$
	High Pressure Sodium								
400 W magnetic	Sunlight Supply	443	416	0.94	$200	2.40	$0.48	$0.35	$0.40
1000 W magnetic	Sunlight Supply	1067	1090	1.02	$275	0.92	$0.25	$0.32	$0.33
1000 W magnetic	PARsource GLXI	1004	1161	1.16	$350	0.86	$0.30	$0.29	$0.31
1000 W electronic	PARsource GLXI	1024	1333	1.30	$380	0.75	$0.29	$0.25	$0.28
1000 W electronic	PARsource GLXII	1026	1334	1.30	$310	0.75	$0.23	$0.25	$0.27
1000 W electronic	Gavita	1033	1751	1.70	$500	0.57	$0.29	$0.19	$0.23
1000 W electronic	ePapillon	1041	1767	1.70	$600	0.57	$0.34	$0.19	$0.24
	LED								
red/ blue	LSG	384	653	1.70	$1,200	1.53	$1.84	$0.19	$0.54
red/ white	BML	326	541	1.66	$1,000	1.85	$1.85	$0.20	$0.54
red / white	LSG	390	634	1.63	$1,200	1.58	$1.89	$0.20	$0.55
red/ white	Illumitex	279	390	1.40	$1,400	2.56	$3.59	$0.24	$0.92
red/ white/ blue	Lumigrow (Pro 325)	304	390	1.29	$1,000	2.56	$2.56	$0.26	$0.73
red/ white	California Lightworks	337	350	1.04	$1,000	2.85	$2.85	$0.32	$0.85
multiple	Black Dog	339	339	1.00	$950	2.95	$2.80	$0.33	$0.85
red/ white	Apache	169	163	0.96	$860	6.14	$5.28	$0.34	$1.35
red/ blue	Lumigrow (ES330)	318	284	0.90	$1,200	3.52	$4.22	$0.37	$1.16
red/ white	Hydrogrow	423	378	0.89	$1,300	2.64	$3.44	$0.37	$1.01
	Ceramic Metal Halide								
315 W 3100 K	Cycloptics	337	491	1.46	$640	2.04	$1.30	$0.23	$0.46
315 W 4200 K	Cycloptics	340	468	1.38	$640	2.14	$1.37	$0.24	$0.48
2@315 W 3100 K	Boulder-lamp	651	817	1.25	$1,000	1.22	$1.22	$0.26	$0.47
	Fluorescent								
400 W induction	iGrow	394	374	0.95	$1,200	2.68	$3.21	$0.35	$0.94
60 W	T8	58	48	0.84	$40	20.77	$0.83	$0.40	$0.51

Table A.4: **Cost per mole photons for four capture assumptions.**

Lamp type and Ballast	Fixture producer	Assuming all radiation (180°) is captured: Fixtures needed per $millimol/J$	Assuming all radiation (180°) is captured: Five year electric cost per Âţmol photons $\$/mol/s\,yr$	Assuming radiation within a 1 to 2.38 height to width ration (100°) is captured: Fixtures needed per $millimol/J$	Assuming radiation within a 1 to 2.38 height to width ration (100°) is captured: Five year electric cost per Âţmol photons $\$/mol/s\,yr$	Assuming radiation within a 1 to 1.35 height to width ration (168°) is captured: Fixtures needed per $millimol/J$	Assuming radiation within a 1 to 1.35 height to width ration (168°) is captured: Five year electric cost per Âţmol photons $\$/mol/s\,yr$
	High Pressure Sodium						
400 W magnetic	Sunlight Supply	2.40	$0.40	3.99	$0.66	8.51	$1.42
1000 W magnetic	Sunlight Supply	0.92	$0.33	1.71	$0.61	3.60	$1.30
1000 W magnetic	PARsource GLXI	0.86	$0.31	1.31	$0.47	2.82	$1.01
1000 W electronic	PARsource GLXI	0.75	$0.28	1.14	$0.42	2.49	$0.92
1000 W electronic	PARsource GLXII	0.75	$0.27	1.33	$0.47	2.81	$1.00
1000 W electronic	Gavita	0.57	$0.23	0.96	$0.38	2.12	$0.84
1000 W electronic	ePapillon	0.57	$0.24	1.46	$0.61	3.47	$1.45
	LED						
red/ blue	LSG	1.53	$0.54	1.62	$0.57	2.03	$0.71
red/ white	BML	1.85	$0.54	2.13	$0.62	3.17	$0.93
red / white	LSG	1.58	$0.55	1.67	$0.59	2.09	$0.73
red/ white	Illumitex	2.56	$0.92	2.66	$0.96	3.82	$1.37
red/ white/ blue	Lumigrow (Pro 325)	2.56	$0.73	3.05	$0.87	4.95	$1.42
red/ white	California Lightworks	2.85	$0.85	3.09	$0.92	4.92	$1.46
multiple	Black Dog	2.95	$0.85	4.43	$1.27	8.64	$2.48
red/ white	Apache	6.14	$1.35	6.58	$1.45	8.21	$1.81
red/ blue	Lumigrow (ES330)	2.64	$1.01	2.82	$1.07	4.33	$1.65
red/ white	Hydrogrow	3.52	$1.16	5.05	$1.67	10.70	$3.54
	Ceramic Metal Halide						
315 W 3100 K	Cycloptics	2.04	$0.46	5.43	$1.22	19.55	$4.38
315 W 4200 K	Cycloptics	2.14	$0.48	5.72	$1.29	20.71	$4.66
2@315 W 3100 K	Boulder-lamp	1.22	$0.47	1.56	$0.60	2.90	$1.12
	Fluorescent						
400 W induction	iGrow	2.68	$0.94	4.69	$1.65	10.17	$3.58
60 W	T8	20.77	$0.51	38.03	$0.93	83.81	$2.05

Appendix A References

, I.T.P.C.. IES Approved Method for the Electrical and Photometric Measurements of Solid-state Lighting Products. Illuminating Engineering Society, 2008.

Blonquist, M., Bugbee, B.. Analysis of spectral and cosine errors in quantum sensors. In: NCERA 101. West Lafayette, IN; 2013. URL: http://www.apogeeinstruments.com/content/Quantum-Sensor-Poster-Park-City-April-2009.pdf.

Both, A.J., Ciolkosz, D.E., Albright, L.D.. Evaluation of light uniformity underneath supplemental lighting systems. Acta Hort (ISHS) 2000;580:183–190. URL: http://www.actahort.org/books/580/580_23.htm.

Bourget, C.M.. An introduction to light-emitting diodes. HortScience 2008;43(7):1944–1946. URL: http://hortsci.ashspublications.org/content/43/7/1944.short.

Ciolkosz, D.E., Both, A.J., Albright, L.D.. Selection and placement of greenhouse luminaires for uniformity. Applied Engineering in Agriculture 2001;17(6). URL: http://elibrary.asabe.org/abstract.asp??JID=3&AID=6842&CID=aeaj2001&v=17&i=6&T=1. doi:10.13031/2013.6842.

Cope, K.R., Bugbee, B.. Spectral effects of three types of white light-emitting diodes on plant growth and development: Absolute versus relative amounts of blue light. HortScience 2013;48(4):504–509.

Cope, K.R., Snowden, M.C., Bugbee, B.. Photobiological Interactions of Blue Light and Photosynthetic Photon Flux: Effects of Monochromatic and Broad-Spectrum Light Sources. Photochemistry and Photobiology 2014;90(3):574–584. URL: http://doi.wiley.com/10.1111/php.12233. doi:10.1111/php.12233.

Craig, D.S., Runkle, E.S.. A Moderate to High Red to Far-red Light Ratio from Light-emitting Diodes Controls Flowering of Short-day Plants. Journal of the American Society for Horticultural Science 2013;138(3):167–172. URL: http://journal.ashspublications.org/content/138/3/167.short.

Dougher, T.A., Bugbee, B.. Differences in the Response of Wheat, Soybean and Lettuce to Reduced Blue Radiation. Photochemistry and photobiology 2001;73(2):199–207.

Dougher, T.A., Bugbee, B.. Long-term blue light effects on the histology of lettuce and soybean leaves and stems. Journal of the American Society for Horticultural Science 2004;129(4):467–472.

Ferentinos, K., Albright, L.. Optimal design of plant lighting system by genetic algorithms. Engineering Applications of Artificial Intelligence 2005;18(4):473–484. URL: http://linkinghub.elsevier.com/retrieve/pii/S0952197604001654. doi:10.1016/j.engappai.2004.11.005.

Gómez, C., Morrow, R.C., Bourget, C.M., Massa, G.D., Mitchell, C.A.. Comparison of intracanopy light-emitting diode towers and overhead high-pressure sodium lamps for supplemental lighting of greenhouse-grown tomatoes. HortTechnology 2013;23(1):93–98. URL: http://horttech.ashspublications.org/content/23/1/93.short.

Inada, K.. Action spectra for photosynthesis in higher plants. Plant and Cell Physiology 1976;17(2):355–365.

Johkan, M., Shoji, K., Goto, F., Hahida, S., Yoshihara, T.. Effect of green light wavelength and intensity on photomorphogenesis and photosynthesis in Lactuca sativa. Environmental and Experimental Botany 2012;75:128–133. URL: http://linkinghub.elsevier.com/retrieve/pii/S0098847211001924. doi:10.1016/j.envexpbot.2011.08.010.

Kim, H.H., Goins, G.D., Wheeler, R.M., Sager, J.C.. Green-light supplementation for enhanced lettuce growth under red-and blue-light-emitting diodes. HortScience 2004;39(7):1617–1622.

Massa, G.D., Kim, H.H., Wheeler, R.M., Mitchell, C.A.. Plant productivity in response to LED lighting. HortScience 2008;43(7):1951–1956. URL: http://hortsci.ashspublications.org/content/43/7/1951.short.

McCree, K.. The action spectrum, absorptance and quantum yield of photosynthesis in crop plants. Agricultural Meteorology 1972;9(0):191–216. URL: http://www.sciencedirect.com/science/article/pii/0002157171900227. doi:10.1016/0002-1571(71)90022-7.

Morrow, R.C.. LED lighting in horticulture. HortScience 2008;43(7):1947–1950. URL: http://hortsci.ashspublications.org/content/43/7/1947.short.

Morrow, R.C., Tibbitts, T.W.. Evidence for involvement of phytochrome in tumor development on plants. Plant physiology 1988;88(4):1110–1114. URL: http://www.plantphysiol.org/content/88/4/1110.short.

Nelson, J.A., Bugbee, B.. Spectral characteristics of lamp types for plant biology. In: NCERA 101. West Lafayette, IN; 2013. URL: http://cpl.usu.edu/files/publications/poster/pub__6740181.pdf.

Yang, Z.C., Kubota, C., Chia, P.L., Kacira, M.. Effect of end-of-day far-red light from a movable LED fixture on squash rootstock hypocotyl elongation. Scientia Horticulturae 2012;136:81–86. URL: http://linkinghub.elsevier.com/retrieve/pii/S0304423811006698. doi:10.1016/j.scienta.2011.12.023.

Yorio, N.C., Goins, G.D., Kagie, H.R., Wheeler, R.M., Sager, J.C.. Improving spinach, radish, and lettuce growth under red light-emitting diodes (LEDs) with blue light supplementation. HortScience 2001;36(2):380–383. URL: http://hortsci.ashspublications.org/content/36/2/380.short.

Appendix B

Analysis of environmental effects on leaf temperature under sunlight, High Pressure Sodium and Light Emitting Diodes

Abstract. The use of LED technology is commonly assumed to result in significantly cooler leaf temperatures than high pressure sodium technology. To evaluate the magnitude of this effect, we measured radiation incident to and absorbed by a leaf under four radiation sources: clear sky sunlight in the field, sunlight in a glass greenhouse, and indoor plants under either high pressure sodium or light emitting diodes. We then applied a common mechanistic energy-balance model to compare leaf to air temperature difference among the radiation sources and environments. At equal photosynthetic photon flux, our results indicate that the effect of plant water status and leaf evaporative cooling is much larger than the effect of radiation source. If plants are not water stressed, leaves in all four radiation sources were typically within 2°of air temperature. Under clear sky conditions, cool sky temperatures mean that leaves in the field are always cooler than greenhouse or indoor plants-when photosynthetic photon flux, stomatal conductance, wind speed, vapor pressure deficit, and leaf size are equivalent. As water stress increases and cooling via transpiration decreases, leaf temperatures can increase well above air temperature. In a near-worst case scenario of water stress and low wind, our model indicates that leaves would increase 6°, 8°, 10°, and 12 above air temperature under field, LED, greenhouse, and HPS scenarios, respectively. Because LED fixtures emit much of their heat through convection rather than radiative cooling, they result in slightly cooler leaf temperatures than leaves in greenhouses and under HPS fixtures, but the effect of LED technology on leaf temperature is smaller than is often assumed.

B.1 Introduction

The energy balance of leaves has long been studied in field conditions and a well-developed family of models is used to determine transpiration and leaf temperature over a wide range of environmental conditions, including controlled environments (Baille et al., 1994; Kichah et al., 2012; Seginer, 1984; Shimizu et al., 2004). These models are well developed, and are used to predict values that are hard to measure directly, such as leaf temperature and evapotranspiration (Blonquist et al., 2009). Models also provide the opportunity to compare individual parameters while keeping all other environmental conditions exactly the same. This facilitates comparison of radiation sources.

Although linearization of energy balance models, such as the Penman-Monteith equation, has been widely used, modern computing allows for more precise numerical solutions of leaf temperature. Widmoser (2009) discusses the advantages of using numerical solutions.

A recent analysis showed that the conversion efficiency of electricity to photosynthetic photons of the most efficient commercial scale LED fixtures was equal to the most efficient HPS fixtures at 1.7 μmol photosynthetic photos per joule of electrical input (Nelson and Bugbee, 2014). They thus generate the same amount of thermal energy per photosynthetic photon. LED fixtures, however, dissipate much of their heat away from the plane they illuminate, while HPS fixtures dissipate more heat toward the plane they illuminate.

Elevated temperature reduces the lifespan of LEDs, so they are thermally-bonded to heat sinks where the thermal energy is removed by natural or fan-assisted convection and directed away from the plants they illuminate.

Conversely, HPS lamps operate at higher temperatures and thus generate more longwave radiation in the same direction as the photosynthetic radiation. This thermal radiation can be reduced using a barrier such as glass, but this reduces the photosynthetic radiation by about 10% (Fig. B.1) and thus lowers the efficiency of the fixture.

The difference in how LED and HPS technologies dissipate thermal energy indicates that use of HPS fixtures will result in higher leaf temperatures. It is easy to misjudge the magnitude of this effect because HPS lamps are a far more concentrated light source than LEDs. Comparisons need to be made on the basis of equal photosynthetic photon flux

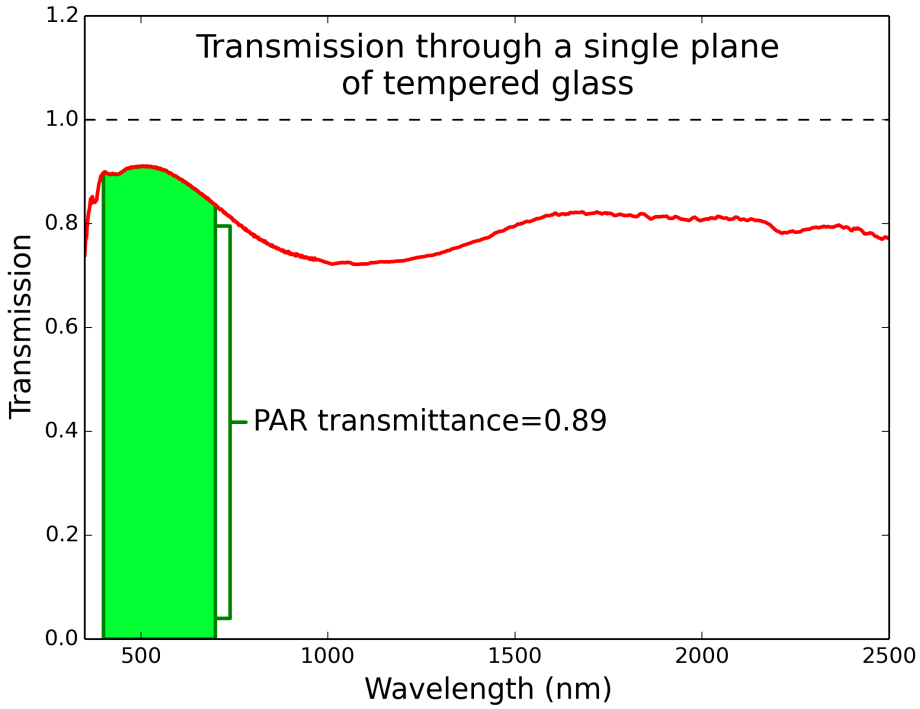

Fig. B.1: **Transmission of radiation through a single pane of tempered glass.** PAR was 89% transmitted.

(PPF).

Compared to sunlight and HPS lamps, LED fixtures emit almost no near infrared radiation (NIR; 700-3000 nm), but this radiation is not well absorbed by plant leaves. Photosynthetic (400 to 700 nm) and longwave (3,000 to 100,000 nm) radiation are about 95% absorbed, but non-photosynthetic solar NIR is only about 20% absorbed, and has a smaller effect on leaf heating. Unabsorbed radiation is either transmitted or reflected.

Our objective was to use a well-established energy-balance model to compare the leaf-to-air temperature difference in four radiation scenarios across multiple environments.

B.2 Materials and Methods

Radiation sources

We made measured the radiation from four sources: clear sky sun in the field, clear sky sun in a greenhouse, and either HPS or LED fixtures in indoor environments (devoid of sunlight). The most efficient at commercially-available HPS and LED fixtures (1.7 $\mu mol/J$;(Nelson and Bugbee, 2014)) were used. The HPS fixture included a double-ended, 1000 W lamp (MASTER GreenPower, Philips Lighting, The Netherlands) in an efficient (less then 10% losses) luminaire (ePapillon, Lights Interaction, The Netherlands). The LED fixture was a 400 W, Red-Blue, passively cooled fixture (VividGro, Lighting Science Group, FL, USA). Clear sky sun measurements were made near solar noon on a clear summer day in Logan, UT, USA. Greenhouse sun measurements were made under clear sky conditions in a typical glass greenhouse.

Absorption of shortwave radiation

We measured shortwave absorption as the fraction of light that is neither transmitted nor reflected by a leaf.

Leaf absorption was determined by measurement of reflection and transmission between 350-2500 nm using a spectroradiometer (FieldSpec Pro, ASD Inc., Boulder, CO, USA) and a halogen light source. Transmission was measured through a single leaf at 90°from the leaf

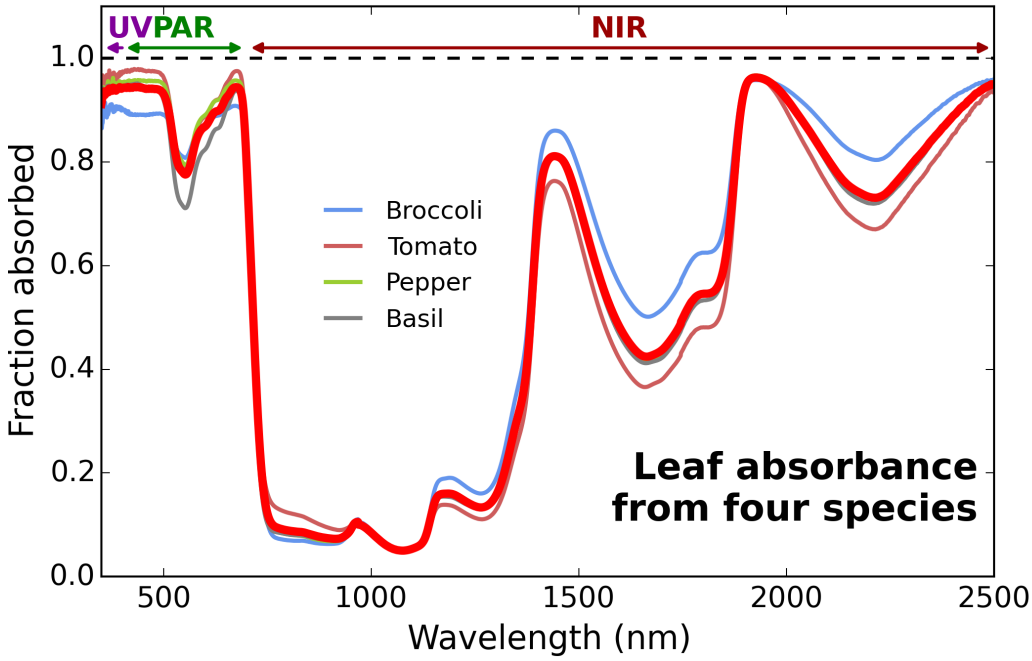

Fig. B.2: **Average absorption (red line) of leaves from tomato, pepper, basil and broccoli.** Variation among species is due to differences in leaf reflectance. The broccoli leaf had slightly higher reflectance of PAR than the other species. All plants were grown in a greenhouse.

surface. Reflectance was made over a large black cavity with a small hole to mimic a black body, again at 90°from the leaf surface. Absorption was averaged among four species: tomato (S. lycopersicum), pepper (C. annuum), basil (O. basilicum), and broccoli (B. oleracea) (Fig. B.2) to incorporate a range of leaf types. Three separate leaves were measured on for each species. Average absorption was nearly identical to previously published values from multiple species and a variety of environments (Jones, 2013; McCree, 1972).

Relative spectral radiance of each radiation source was measured using the same spectro-radiometer as above (Fig. B.3). Incoming shortwave (350-2,500 nm) and longwave (>3,000 nm) radiation measurements for each radiation scenario were made using a net radiometer (CNR1, Kipp & Zonen, the Netherlands). Photosynthetic photon flux (PPF; in moles per m2 per s) measurements were made using a recently calibrated quantum sensor (LI-190, LI-COR, Lincoln, NE, USA), and converted to photosynthetically active radiation (PAR; in watts per m^2) using spectral data for each light source and Planck's equation ($E = hc/\lambda$).

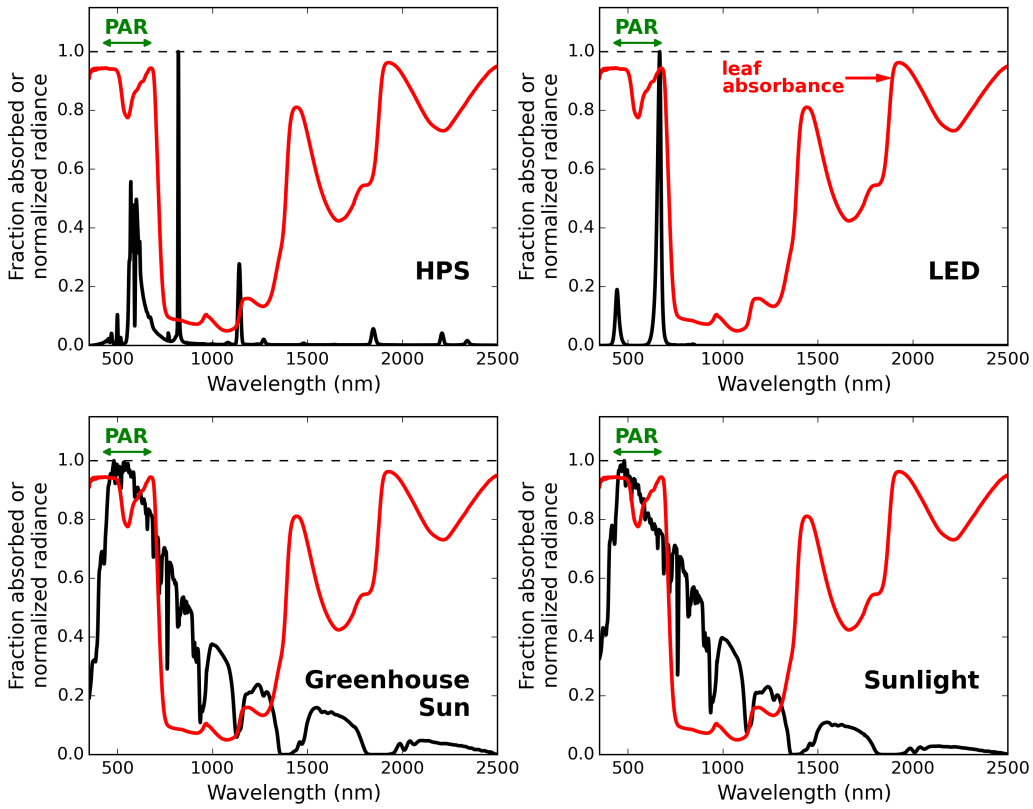

Fig. B.3: **Radiance spectrum from four radiation scources (black line) and average leaf absorbance (red line).** Electric lights (HPS and LED) output most of their radiation in the photosynthetic regions. Sunlight has significant NIR radiation, but this is poorly absorbed by leaves.

The absorbed radiation was normalized to equal incident PPF for each radiation source.

Because, UV and photosynthetic radiation have much higher absorption than NIR, shortwave radiation was divided into three bands: ultraviolet (UV, 350-400 nm), PAR (400-700 nm), and near-infrared (NIR, 700-2500 nm). UV radiation below 350 nm is a minimal component from all radiation sources, and was not included in the analysis.

Incoming and outgoing longwave radiation

Longwave radiation was separated into three components: sky longwave, source longwave, and emitted longwave. Sky longwave is the radiation emitted from either a clear sky (typically 300 W/m^2 or about -1° C), or the ceiling of the controlled environment (as-

sumed to be 452 W/m^2 or about 28° C for all indoor cases). Source longwave is defined as the incoming longwave radiation from either the LED or HPS fixture, and was measured using a black body pyranometer (part of the net radiometer above). Incoming longwave radiation with the fixture present was subtracted from incoming longwave with the fixture absent. Source longwave was scaled with PPF. Emitted longwave is calculated using the Stefan-Boltzman law as outlined below. We assume the leaf is the same temperature as the surfaces below the leaf and thus there is no net longwave transfer.

Energy balance model

We modeled a single top leaf because the uppermost leaves absorb about 75% of the incident radiation and have the greatest temperature differences.

Leaf temperature was calculated using the energy balance model that has been described, in detail, in both Campbell and Norman (1998) and Monteith and Unsworth (1990),

$$R_{abs} = \quad R_{emit} + C + \lambda E \tag{B.1}$$

where,

$$\begin{aligned} R_{abs} &= \text{Absorbed radiation in } {}^{W}\!/_{m^2} \\ R_{emit} &= \text{Emitted radiation via Stefan-Boltzmann law in } {}^{W}\!/_{m^2} \\ C &= \text{Transfer of sensible heat via convection in } {}^{W}\!/_{m^2} \\ \lambda E &= \text{Latent heat transfer in } {}^{W}\!/_{m^2} \end{aligned}$$

Assuming the system is at steady state, the absorbed radiation (R_{abs}) must equal the sum of the emitted radiation (R_{emit}), sensible (C) and latent (λE) heat transfer. Absorbed radiation was measured as described in the previous subsections. Emitted radiation is defined by the Stefan-Boltzmann law,

$$R_{emit} = \varepsilon_s \sigma T_L^4 \tag{B.2}$$

where,

ε_s = Emissivity of the leaf (assumed to be 0.97)

σ = The Stefan-Boltzmann constant or $5.67 * 10^{-8}\, {}^{W}/_{m^2 K^4}$

T_L^4 = Leaf temperature in Kelvin to the fourth power

The transfer of sensible heat (C), through convection, is defined as a function of the difference in leaf to air temperature and the boundary layer conductance such that,

$$C = c_p g_{Ha} (T_L - T_a) \tag{B.3}$$

where,

c_p = Specific heat of air at a constant pressure or $29.3\, {}^{J}/_{mol\ ^\circ C}$

T_L = Leaf temperature in Celsius

T_a = Air temperature in Celsius

Boundary layer conductance (g_{Ha} in ${}^{mol}/_{m^2 s}$) is a semi-empirical function defined as,

$$g_{Ha} = 1.4 * 0.135 \sqrt{\frac{u}{d}} \tag{B.4}$$

where,

1.4 = An empirical constant accounting for turbulance

0.135 = An constant determined by the viscosity, density, and diffusivity of air

u = Wind speed in $^{m}/_{s}$

d = Characteristic dimension in meters or 0.72 times the maximum leaf width

Latent heat transfer (λE) is defined as a function of the vapor pressure deficit ($\frac{e_s(T_L)-e_a}{p_a}$) and the vapor conductance (g_v in $^{mol}/_{m^2 s}$) such that,

$$\lambda E = \lambda g_v \frac{e_s\left(T_L\right) - e_a}{p_a} \tag{B.5}$$

where,

λ = Latent heat of evaporation or $44\,^{kJ}/_{mol}$

$e_s\left(T_L\right)$ = Saturation vapor pressure of water at leaf temperature in kPa

e_a = Partial pressure of water vapor in air in kPa

p_a = Atmospheric pressure or $101.3\,kPa$

Vapor conductance (g_v) is a combination of both the vapor boundary (g_{va}) and stomatal (g_{vs}) conductances (both in c) such that,

$$g_v = \frac{g_{vs} g_{va}}{g_{vs} + g_{va}} \tag{B.6}$$

Stomatal conductance (g_{vs}) typically varies between 0.1 $^{mol}/_{m^2 s}$ for drought stressed plants and 0.5 $^{mol}/_{m^2 s}$ for high transpiring plants. Vapor boundary conductance is defined similarly to equation 4 with slightly different constants,

$$g_{va} = \quad 1.4 * 0.147\sqrt{\frac{u}{d}} \tag{B.7}$$

These components account for all significant energy paths. Other energy sources and sinks include photosynthesis and respiration, which are negligible in these conditions. Combining equations B.1, B.2, B.3, and B.5 gives a comprehensive overview of the model,

$$R_{abs} = \quad \varepsilon_s \sigma T_L^4 + c_p g_{Ha} \left(T_L - T_a\right) + \lambda g_v \frac{e_s \left(T_L\right) - e_a}{p_a} \tag{B.8}$$

The equation was solved for leaf temperature (T_{leaf}) using an iterative approximation. Results are presented as the difference between leaf and air temperature ($T_{leaf} - T_{air}$), as leaf temperature is only relevant in the context of it's environment.

Some of the energy absorbed by leaves is used to fix CO_2 into sucrose in the process of photosynthesis. The photosynthetic energy use in field conditions is typically less than 4% of the total absorbed energy and has thus been ignored in energy balance models. However, assuming optimal water and nitrogen, a moderate PPF and physiologically optimum CO_2 enrichment, it is possible to increase the quantum yield of photosynthesis to 0.08 moles of CO_2 fixed per mole of photons absorbed. Assuming respiration is 30% of photosynthesis, net metabolism can use about 8% of the absorbed shortwave energy (Blonquist et al., 2009). This is still a small contribution to the total energy balance, and it would be similar for all radiation sources.

Code for the execution of the model can be found in supplemental information (File Supporting Information).

Sensitivity analysis

Excluding the radiation inputs, equation 8 is ultimately a function of seven environmental variables: air temperature, relative humidity/vapor pressure deficit, wind speed, leaf size,

sky temperature, stomatal conductance, and atmospheric pressure. Default values for each parameter were chosen to reflect typical growing conditions (as shown in figure captions).

Air temperature was held at 25° C, which is a common set point for greenhouses and growth chambers. Convective heat transfer from the lighting fixture and surrounding air is assumed to be controlled via the temperature control system before it would impact leaf temperature. When other environmental conditions are constant, air temperature between 15°and 35° C has a minimal effect on leaf to air difference (Fig. B.4).

Environmental parameters were varied across a biologically significant range.

B.3 Results and discussion

The greatest variation among sources in incident radiation was in the near-infrared (NIR) and longwave bands (Table B.1). NIR is poorly absorbed by leaves, so absorbed NIR was less than 30% of absorbed PAR energy for all sources.

The indoor environments (LED, HPS, and greenhouse) had net positive longwave radiation, and the HPS fixture was significantly higher than the other sources. The effect of UV on absorbed radiation was less than 10% of absorbed PAR energy for all source.

Effect of environment on leaf to air temperature difference

The leaf-to-air temperature difference, in all radiation scenarios, was less than 2° C except where parameters approached their extremes (Fig. B.5). The relative order did not change, regardless of environmental conditions, with HPS > greenhouse sun > LED > clear sky sunlight.

Near worst-case conditions (water stress, high PPF, and low wind; Fig. B.6) increased the differences between lighting sources. The results indicate that leaf temperatures in near worst-case conditions can increase 6°to 12° C above air temperature depending on the radiation scenario.

Differences in radiation absorption

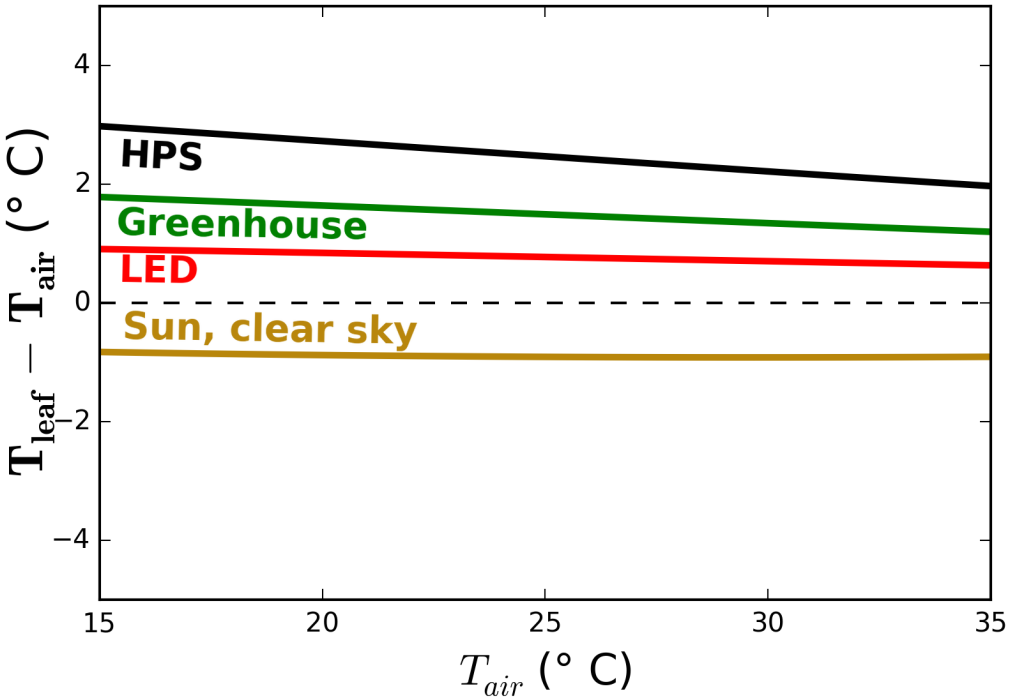

Environmental parameters:

Stomatal conductance	= 0.4 $moles/m^2\,s$
Wind speed	= 1.0 m/s
Leaf width	= 5 cm
Vapor pressure deficit	= 1.6 kPa
Photosynthetic photon flux (PPF)	=1000 $\mu moles/m^2\,s$

Fig. B.4: **Leaf temperature response to air temperature.** Vapor pressure deficit was held constant.

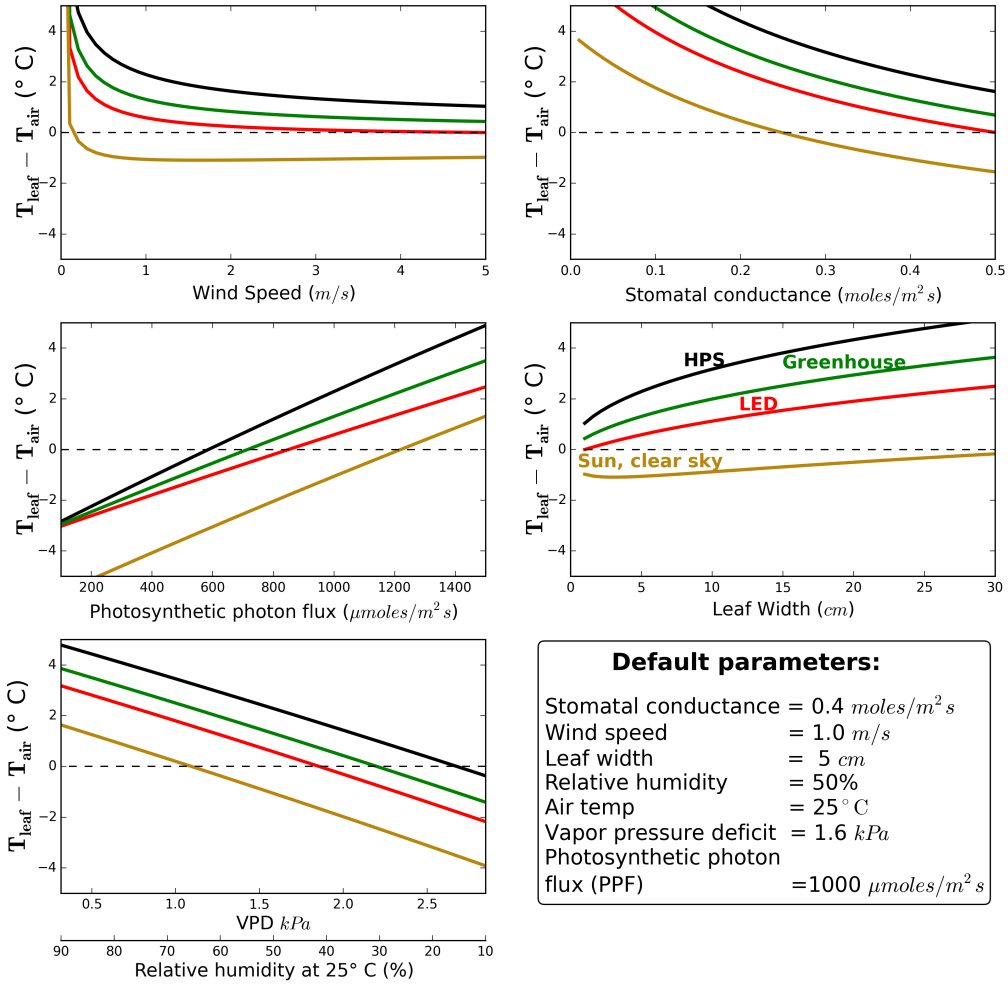

Fig. B.5: **Radiance spectrum from four radiation scources (black line) and average leaf absorbance (red line).** Electric lights (HPS and LED) output most of their radiation in the photosynthetic regions. Sunlight has significant NIR radiation, but this is poorly absorbed by leaves.

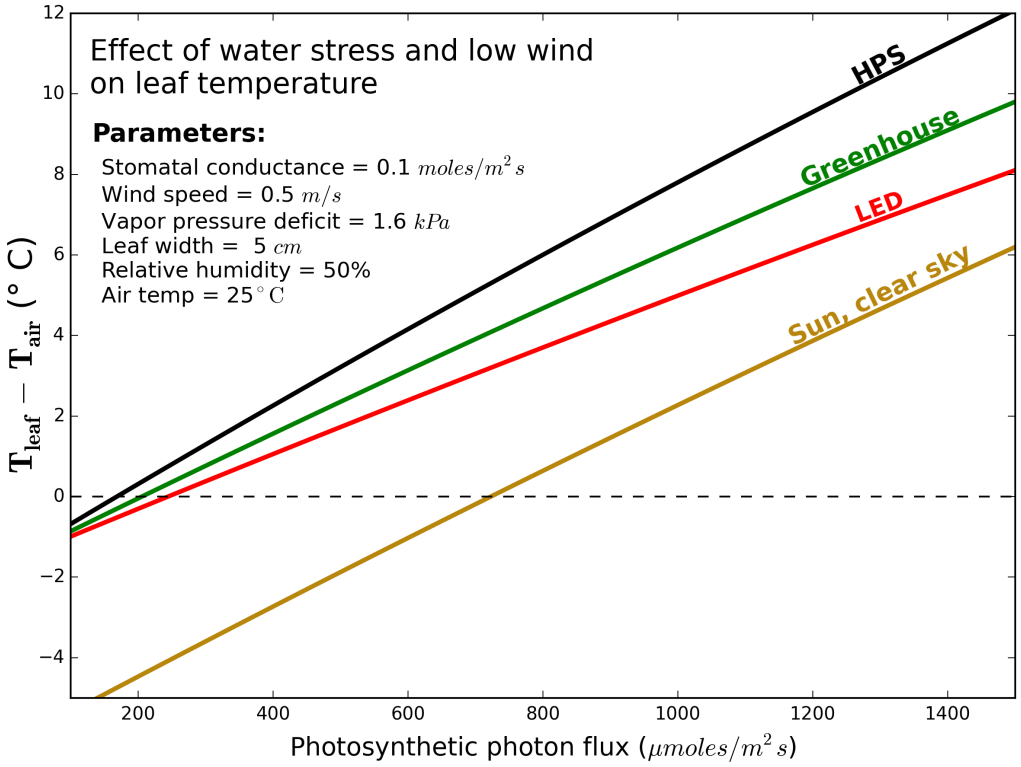

Fig. B.6: **Calculated effects of PPF on the difference between leaf temperature and air temperature under four radiation scenarios in near worst-case conditions of water stress and low wind.**

Table B.1: **Incident radiation, fraction absorbed, and total absorbed radiation for each source.** The absorbed radiation was normalized to a PPF of 1000 µmoles per m^2 per s for each radiation source. This does not result in exactly equal PAR (in watts per m^2) because of spectral differences among radiation sources. The total absorbed radiation for each source is shown in bold. Leaf temperature was held constant at 25° C. Net longwave exchange with lower leaves or surfaces was assumed to be zero.

	UV (350-400 nm)	PAR (400-700 nm)	NIR (700-2500 nm)	Source longwave	Sky longwave	Emitted longwave	Total
	Incident radiation (W/m^2)						
HPS	0.58	203	128	131	452	-435	480
LED	0.15	195	10	44	452	-435	267
Sun, greenhouse	18	219	252	0	452	-435	508
Sun, clear sky	19	219	288	0	300	-435	392
	Fraction absorbed						
HPS	0.939	0.870	0.263	0.97	0.97	0.97	0.71
LED	0.934	0.943	0.923	0.97	0.97	0.97	0.90
Sun, greenhouse	0.938	0.894	0.214	0.97	0.97	0.97	0.53
Sun, clear sky	0.937	0.894	0.207	0.97	0.97	0.97	0.33
	Total absorbed radiation (W/m^2)						
HPS	0.54	177	34	127	439	-422	**342**
LED	0.14	184	9	43	439	-422	**240**
Sun, greenhouse	17	196	54	0	439	-422	**271**
Sun, clear sky	18	196	60	0	291	-422	**130**

There were significant differences among sources in the ratio of NIR to PPF, but NIR wavelengths are poorly absorbed by leaves (Table B.1), thus the effect of NIR on leaf temperature is relatively small. Blanchard and Runkle (2010) found leaf temperature to be 0.7°to 1.5° C lower under NIR reflective painted glass as opposed to neutral reflective painted glass with similar PPF conditions (about 1100 $\mu mole/m^2 s$), though much of this difference was likely due to differences in air temperature, which was on average 0.8° C higher under neutral reflective paint. This further shows that though NIR is a significant source of energy, it's

impact on individual leaves is small.

Longwave radiation varied significantly among radiation sources and had the biggest effect on leaf temperature. Because incoming longwave radiation from clear sky conditions is significantly less than that from the ceiling of controlled environments, plants grown outdoors have lower absorbed net radiation. Even on overcast days, incoming long wave radiation in the field is typically lower than in a controlled environment.

Our analysis includes two of the most efficient fixtures available. Increases or decreases in efficiency will likely cause small differences in source longwave radiation, but the effect of changes in fixture efficiency would be relatively small compared to the effect of differences between the two technologies.

Effect of light source on transpiration

Increased leaf temperature causes increased transpiration. When incoming radiation and radiation capture by the crop are the same, the transpiration rate of crops in protected environments are thus higher than the same crops the field.

In the field, however, water loss by evaporation from the soil surface can make the combination of evaporation and transpiration higher than the combination of evaporation and transpiration in a controlled environment. If the effect of surface evaporation is removed and transpiration from only the leaves is considered, crops in a greenhouse would have a 35% higher transpiration rate than identical crops grown in the field.

Based on our presented model and the default parameters (Fig B.5), the reduced leaf temperature under LED fixtures would decrease transpiration by 17% compared to HPS fixtures. This is a potentially significant reduction in transpiration, but differences in surface evaporation among cultural systems typically have a greater effect on crop water requirement than lamp type. For example, drip irrigation can decrease evaporation from surfaces and reduce the crop water requirement by 30 to 70%, in both greenhouses and in the field (Camp, 1998).

Effect of elevated CO_2

Controlled environments often add supplemental CO_2, which can decrease stomatal conductance 10-40% (Ainsworth and Rogers, 2007; Wheeler et al., 1999), and increase leaf temperature. The presented model indicates that a decrease in stomatal conductance of 30% in response to elevated CO_2 would increase leaf temperature by 1° C in all radiation scenarios.

Effect of light source on shoot tip temperature

Shoot tip temperature is often used to predict time to flower and plant development rates (Faust and Heins, 1993). Our modeling approach is similar to that used by Shimizu et al. (2004) and Faust and Heins (1998) to predict shoot tip temperature, both of which found greater than 83% of their modeled values to be within 1° C of measured values. Because our models are similar, choice of lighting technology will likely affect shoot tip temperature, time to flower and plant development.

Effect of light source on fruit and flower temperature

Our near-worst case analysis would likely be representative of flowers, fruits, and thick, dense plant parts that have low transpiration rates, including high value products such as tomatoes, strawberries, and *Cannabis* flowers. These thicker structures would absorb more radiation than a thin leaf. Our measurements show that while only 63% of HPS shortwave radiation is absorbed by the first leaf, a structure ten times thinker would absorb more than 80%. LED technology has the potential to reduce heating of these thick, low transpiring plant structures.

B.4 Conclusions

The presented model indicates that the use of LED technology reduces leaf temperature by about 1.3° C compared to HPS technology under typical growing conditions, but a leaf in a controlled environment will be warmer than a leaf in the field under a clear sky, assuming equal PPF and similar environmental conditions. In conditions where leaves benefit from heating, such as a greenhouse in a cool climate, HPS technology more effectively transfers

heat to canopies.

B.5 Supporting Information

[Overview of code used to run the associated model] Overview of code used to run the associated model.

```
#Variables
u = 1.5 #wind speed m/s
dmax = 10 #maximum length of leaf in cm
d = 0.72*(dmax/100) #characteristic dimension
hr = 0.5 #relative humidity
Rabs = 750 #radiation absorbed in W/m2
Tcel = 25 #air temperature is celcius
Tkel = Tcel+273.15
pa = 100 #air pressure in kPa
gvsab = 0.5 #stomatal conductace for vapor abaxial side, ranges from 0.01 to 0.5
gvsad = 0.5 #stomatal conductace for vapor adaxial side, ranges from 0.01 to 0.5
gvs=0.25

#Constants
lam = 44000 #lambda-the latent heat of evaporation J/molC
Cp = 29.3 #Cp-specific heat of air J/molC
a = 0.611 #SVP constant
b = 17.502 #SVP constant
c = 240.97 #SVP constant
sig = 5.67E-8 #sigma-Stephan Boltzman constant W/m2k4
eps = 0.97 #epsilon sub s-Emissivity of leaf
gamma = Cp/lam
```

```
#s-slope of saturation mole fraction function
def esfun(Tcel):
    a = 0.611 #SVP constant
    b = 17.502 #SVP constant
    c = 240.97 #SVP constant
    es = a*np.exp((b*Tcel)/(Tcel+c))
    return(es)

#slope of saturation mole fraction function: Tcel = air temp in celcius, pa =
    atmospheric pressure in kPa
def sfun(Tcel,pa):
    a = 0.611 #SVP constant
    b = 17.502 #SVP constant
    c = 240.97 #SVP constant
    es=esfun(Tcel)
    delta = (b*c*es)/(c+Tcel)**2
    return(delta/pa)

#gHr-boundry layer conductance for heat

def grfun(Tcel): #radiative conductance: Tcel = air temp in celcius
    Tkel = Tcel+273.15
    gr = (4*eps*sig*Tkel**3)/Cp
    return(gr)

def gHafun(u,d): #boundry layer conductance for heat: u = wind speed, d =
    characteristic dimension
    gHa = 0.135*np.sqrt(u/d)
    return(gHa)

gHr = grfun(Tcel)+gHafun(u,d)
```

```
##gv-conductance for vapor
def  gvafun(u,d): #boundry layer conductance for vapor: u = wind speed, d =
    characteristic dimension
    gva = 0.147*np.sqrt(u/d)
    return(gva)

def gvfun(gvsab,gvsad,gva): #conductance for vapor
    gvab = (0.5*gvsab*gva)/(gvsab+gva) #conductance of vapor from abaxial side
    gvad = (0.5*gvsad*gva)/(gvsad+gva) #conductance of vapor from adaxial side
    gv = gvab+gvad
    return(gv)



def TLitt(Rabs,Tcel,gvs,u,d,hr,pa):
    ea=esfun(Tcel)*hr
    Rabs=Rabs
    Tcel=Tcel
    gvs=gvs
    u=u
    d=d
    hr=hr
    pa=pa

    def TLinfun(x):
        #constants
        lam = 44000 #lambda-the latent heat of evaporation J/molC
        Cp = 29.3 #Cp-specific heat of air J/molC
        sig = 5.67E-8 #sigma-Stephan Boltzman constant W/m2k4
        eps = 0.97 #epsilon sub s-Emissivity of leaf

        #functions
        gHa = 1.4*gHafun(u,d)
```

```
    gva = 1.4*gvafun(u,d)
    gv = (gvs*gva)/(gvs+gva)
    xkel=x+273.15

    return(Rabs-eps*sig*(xkel**4)-Cp*gHa*(x-Tcel)-lam*gv*((esfun(x)-ea)/pa))

TLit = fsolve(TLinfun,TLfun(Rabs,Tcel,gvs,u,d,hr,pa))
return(TLit)
```

Appendix B References

Ainsworth, E.A., Rogers, A.. The response of photosynthesis and stomatal conductance to rising CO_2: mechanisms and environmental interactions: Photosynthesis and stomatal conductance responses to rising CO_2. Plant, Cell & Environment 2007;30(3):258–270. URL: http://doi.wiley.com/10.1111/j.1365-3040.2007.01641.x. doi:10.1111/j.1365-3040.2007.01641.x.

Baille, M., Baille, A., Delmon, D.. Microclimate and transpiration of greenhouse rose crops. Agricultural and Forest Meteorology 1994;71(1–2):83–97. URL: http://www.sciencedirect.com/science/article/pii/0168192394901015. doi:10.1016/0168-1923(94)90101-5.

Blanchard, M.G., Runkle, E.S.. Influence of NIR-reflecting shading paint on greenhouse environment, plant temperature, and growth and flowering of bedding plants. Transactions of the ASABE 2010;53(3):939–944.

Blonquist, J., Norman, J., Bugbee, B.. Automated measurement of canopy stomatal conductance based on infrared temperature. Agricultural and Forest Meteorology 2009;149(12):2183–2197. URL: http://linkinghub.elsevier.com/retrieve/pii/S0168192309002329. doi:10.1016/j.agrformet.2009.10.003.

Camp, C.R.. Subsurface drip irrigation: a review. Transactions of the ASAE 1998;41(5):1353–1367.

Campbell, G.S., Norman, J.M.. An introduction to environmental biophysics. Springer, 1998.

Faust, J.E., Heins, R.D.. Modeling leaf development of the African violet (Saintpaulia ionantha Wendl.). Journal of the American Society for Horticultural Science 1993;118(6):747–751. URL: http://journal.ashspublications.org/content/118/6/747.short.

Faust, J.E., Heins, R.D.. Modeling shoot-tip temperature in the greenhouse environment. Journal of the American Society for Horticultural Science 1998;123(2):208–214.

Jones, H.G.. Plants and microclimate: a quantitative approach to environmental plant physiology. Cambridge University Press, 2013.

Kichah, A., Bournet, P.E., Migeon, C., Boulard, T.. Measurement and CFD simulation of microclimate characteristics and transpiration of an Impatiens pot plant crop in a greenhouse. Biosystems Engineering 2012;112(1):22–34. URL: http://linkinghub.elsevier.com/retrieve/pii/S1537511012000207. doi:10.1016/j.biosystemseng.2012.01.012.

McCree, K.. The action spectrum, absorptance and quantum yield of photosynthesis in crop plants. Agricultural Meteorology 1972;9(0):191–216. URL: http://www.sciencedirect.com/science/article/pii/0002157171900227. doi:10.1016/0002-1571(71)90022-7.

Monteith, J.L., Unsworth, M.H.. Principles of environmental physics. 2nd ed. Edward Arnald, 1990.

Nelson, J.A., Bugbee, B.. Economic analysis of greenhouse lighting: light emitting diodes vs. high intensity discharge fixtures. PLoS ONE 2014;9(6):e99010. URL: http://dx.plos.org/10.1371/journal.pone.0099010. doi:10.1371/journal.pone.0099010.

Seginer, I.. On the night transpiration of greenhouse roses under glass or plastic cover. Agricultural Meteorology 1984;30(4):257–268. URL: http://www.sciencedirect.com/science/article/pii/0002157184900025. doi:10.1016/0002-1571(84)90002-5.

Shimizu, H., Runkle, E.S., Heins, R.D.. A steady-state model for prediction of poinsettia plant shoot-tip temperature. Journal of the American Society for Horticultural Science 2004;129(3):303–312.

Wheeler, R.M., Mackowiak, C.L., Yorio, N.C., Sager, J.C.. Effects of CO_2 on stomatal conductance: do stomata open at very high CO_2 concentrations? Annals of botany 1999;83(3):243–251. URL: http://aob.oxfordjournals.org/content/83/3/243.short.

Widmoser, P.. A discussion on and alternative to the Penman–Monteith equation. Agricultural Water Management 2009;96(4):711–721. URL: http://linkinghub.elsevier.com/retrieve/pii/S0378377408002643. doi:10.1016/j.agwat.2008.10.003.